

Supporting Information

Additive-Free, Cost-Effective Hole-Transporting Materials for Perovskite Solar Cells Based on Vinyl Triarylamines

Hidetaka Nishimura,^{*,†} Iku Okada,[†] Taro Tanabe,[†] Tomoya Nakamura,[‡] Richard Murdey,[‡] and Atsushi Wakamiya^{*,‡}

[†]*Fine Chemicals R&D, Toda Research Center, Tokyo Chemical Industry Co., Ltd., Toda, Saitama 335-0033, Japan*

[‡]*Institute for Chemical Research, Kyoto University, Uji, Kyoto 611-0011, Japan*

*E-mail: hidetaka.nishimura@tcichemicals.com; wakamiya@scl.kyoto-u.ac.jp

Table of Contents

- General	S2
- Computation method	S3
- Synthesis	S4
- DFT calculations	S6
- Cyclic voltammograms	S9
- Photophysical properties	S11
- Ionization potentials	S12
- Thermal properties	S15
- Estimation of hole mobilities and conductivities	S18
- Steady-state and time-resolved photoluminescence measurements	S20
- Preparation of perovskite solar cells	S22
- Solar cell device performances	S24
- SEM images	S30
- References	S35
- NMR spectra	S36

General

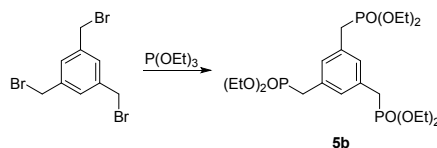
Thin layer chromatography (TLC) was performed on plates coated with 0.25 mm thick silica gel 60F-254 (Merck). Column chromatography was performed using PSQ 100B (TCI). Melting points (mp) were measured on a Yanaco Micro Melting Point Apparatus. ^1H and ^{13}C NMR spectra were recorded with a JEOL ECA 400 (400 MHz for ^1H and 100 MHz for ^{13}C) spectrometers. The NMR chemical shifts are reported in ppm with reference to residual protons and carbons of CDCl_3 (δ 7.26 ppm in ^1H NMR, δ 77.0 ppm in ^{13}C NMR) and CD_2Cl_2 (δ 5.32 ppm in ^1H NMR, δ 53.8 ppm in ^{13}C NMR). Cyclic voltammetry (CV) was performed on an ALS/chi-660E electrochemical analyzer. The CV cell consisted of a glassy carbon electrode, a Pt wire counter electrode, and an Ag/AgNO_3 reference electrode. The measurement was carried out under an argon atmosphere using CH_2Cl_2 solutions of samples (1 mM) with 0.1 M tetrabutylammonium hexafluorophosphate ($\text{Bu}_4\text{N}^+\text{PF}_6^-$) as a supporting electrolyte. UV-vis absorption measurement was performed with a Shimadzu UV-3150 spectrometer (Shimadzu Co.), in degassed spectral grade solvents. Fluorescence measurement was performed with a FluoroMax 4P-NIR (Horiba, Ltd). Quantum yields were determined with a Quantaurus QY C11347 (Hamamatsu Photonics Co., Ltd.) with calibrated integrating sphere system. The HOMO energy levels in the solid state were determined from the onset of photoelectron spectra measured with a photoelectron yield spectrometer under vacuum, model BIP-KV-201-P5 (Bunkoukeiki Co., Ltd.). Thermogravimetric analysis (TGA) was performed on a Thermoplus TG-8120 apparatus (Rigaku Co.). The values are given for a weight-loss of 5% (T_{d5}). Differential scanning calorimetry (DSC) was performed on a DSC-60 apparatus (Shimadzu Co.). All reactions were carried out under an N_2 atmosphere. For the time-resolved photoluminescence (TRPL) measurements, the samples were excited by a picosecond pulsed light with a wavelength of 688 nm (Advanced Laser Diode System). The excitation fluence was set at 127 nJ/cm^2 . The PL signals were recorded using an avalanche photodiode (ID Quantique) and a time-correlated single photon counting board (Becker and Hickl). The PL lifetimes were obtained by fitting the PL decay curve with an exponential function. The PL spectra were recorded using an InGaAs array detector equipped with a monochromator (Princeton Instruments). The samples were kept in an Ar-filled metallic box for the whole process to avoid oxygen contamination and degradation. Current-voltage measurements (J - V curves) for perovskite solar cells were measured in air with an OTENTO-SUNIII (Bunkoukeiki Co., Ltd.) and a Keithley 2400. Incident photon to current efficiency (IPCE) spectra were recorded on a SMO-250III (Bunkoukeiki Co., Ltd.). The light intensity of the illumination source was adjusted by using standard silicon photodiodes: BS520 for J - V characteristics and SiPD S1337-1010BQ for IPCE measurements, respectively. The photo stability for solar cells were measured using a BIR-50P1 (Bunkoukeiki Co., Ltd.).

Computation method

DFT calculations for optimization of the geometries were conducted using the Gaussian 09 program.¹

Synthesis

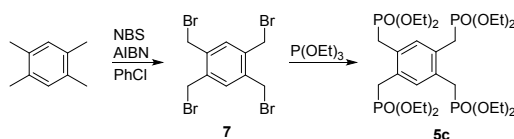
Scheme S1. Synthesis of 1,3,5-tris(diethoxyphosphorylmethyl)benzene (**5b**).



1,3,5-Tris(bromomethyl)benzene (2.50 g, 7.01 mmol) and triethyl phosphite (5.5 mL, 31.8 mmol) were mixed and stirred at 130 °C for 1 h. The formed ethyl bromide was collected by a distillation apparatus. The reaction mixture was concentrated under reduced pressure at 100 °C to give 3.46 g (6.55 mmol) of **5b** in 93% yield as pale yellow oil.

¹H NMR (400 MHz, CDCl₃): δ 7.13 (m, 3H), 4.02 (m, 12H), 3.11 (d, ³J(H,P) = 22.8 Hz, 6H), 1.25 (t, ³J(H,H) = 6.8 Hz, 18H).

Scheme S2. Synthesis of 1,2,4,5-tetrakis(diethoxyphosphorylmethyl)benzene (**5c**).



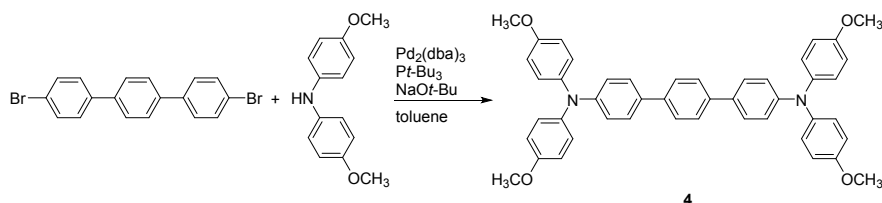
1,2,4,5-Tetrakis(bromomethyl)benzene (7). 1,2,4,5-Tetramethylbenzene (5.37 g, 40.0 mmol) was dissolved in ethyl acetate (120 mL). *N*-Bromosuccinimide (32.0 g, 180 mmol) and AIBN (330 mg, 2.01 mmol) were added to the solution and the solution was stirred at 70 °C for 2 h. The reaction mixture was cooled to room temperature and insoluble materials were filtered off and the filtrate was concentrated under reduced pressure. The obtained crude product was washed with methanol (80 mL) and recrystallized by toluene (30 mL) to give 6.27 g (13.9 mmol) of **7** in 35% yield as white solid.

¹H NMR (400 MHz, CDCl₃) δ 7.37 (s, 2H), 4.60 (s, 8H).

1,2,4,5-Tetrakis(diethoxyphosphorylmethyl)benzene (5c). **7** (4.50 g, 10.0 mmol) and triethyl phosphite (10.3 mL, 60.0 mmol) were mixed and stirred at 130 °C for 1 h. The formed ethyl bromide was collected by a distillation apparatus. The reaction mixture was concentrated under reduced pressure at 130 °C to obtain colorless oil. Hexane (10 mL) was added to the oil and stirred to obtain white solid. The obtained solid was collected by filtration and washed with hexane to give 6.61 g (9.74 mmol) of **5c** in 97% yield as white solid.

^1H NMR (400 MHz, CDCl_3) δ 7.14 (s, 2H), 3.97 (m, 16H), 3.34 (d, $^3J(\text{H,P}) = 19.6$ Hz, 8H), 1.21 (t, $^3J(\text{H,H}) = 7.2$ Hz, 24H).

Scheme S3. Synthesis of 4-(methoxy)-*N*-(4-(methoxy)phenyl)-*N*-phenylaniline (**4**).



4,4''-Dibromo-*p*-terphenyl (2.09 g 5.38 mmol), 4,4'-dimethoxydiphenylamine (2.49 g 10.9 mmol), tris(dibenzylideneacetone)dipalladium(0) (75 mg, 0.082 mmol), and sodium *tert*-butoxide (1.56 g, 16.2 mmol) were charged in a two-neck flask. Tri-*tert*-butylphosphine (69 mg, 0.34 mmol), and toluene (50 mL) were charged in the flask and the mixture was stirred at 90 °C for 5 h. The reaction mixture was quenched by water (50 mL). The organic phase was extracted with toluene (20 mL \times 3), washed by brine (40 mL) and dried over MgSO_4 . MgSO_4 was filtered off and filtrate was concentrated under reduced pressure. The obtained crude product was passed through a short pad of silica gel with the eluent of CH_2Cl_2 and further purified by silica gel column chromatography (toluene) to give 2.89 g (4.22 mmol) of **4** in 78% yield as pale yellow solid.

mp: 193.1–194.8 °C; ^1H NMR (400 MHz, CD_2Cl_2): δ 7.60 (s, 4H), 7.47 (d, $^3J(\text{H,H}) = 8.8$ Hz, 4H), 7.08 (d, $^3J(\text{H,H}) = 8.4$ Hz, 8H), 6.97 (d, $^3J(\text{H,H}) = 8.8$ Hz, 4H), 6.86 (d, $^3J(\text{H,H}) = 8.8$ Hz, 8H), 3.7 (s, 12H).

DFT calculations

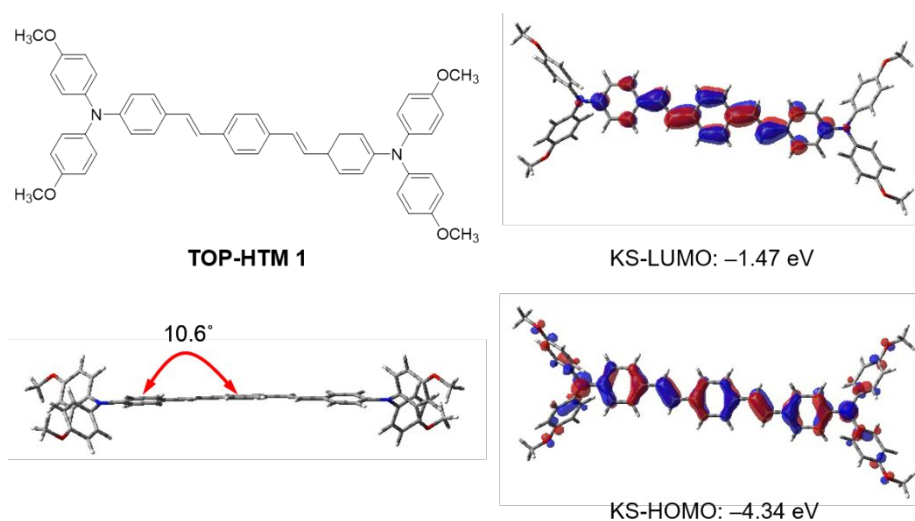


Figure S1. Optimized molecular geometries determined at the B3LYP/6-31G(d) level of theory and pictorial presentation of the frontier orbitals, a plot of the Kohn-Sham HOMO and LUMO energy levels for TOP-HTM 1.

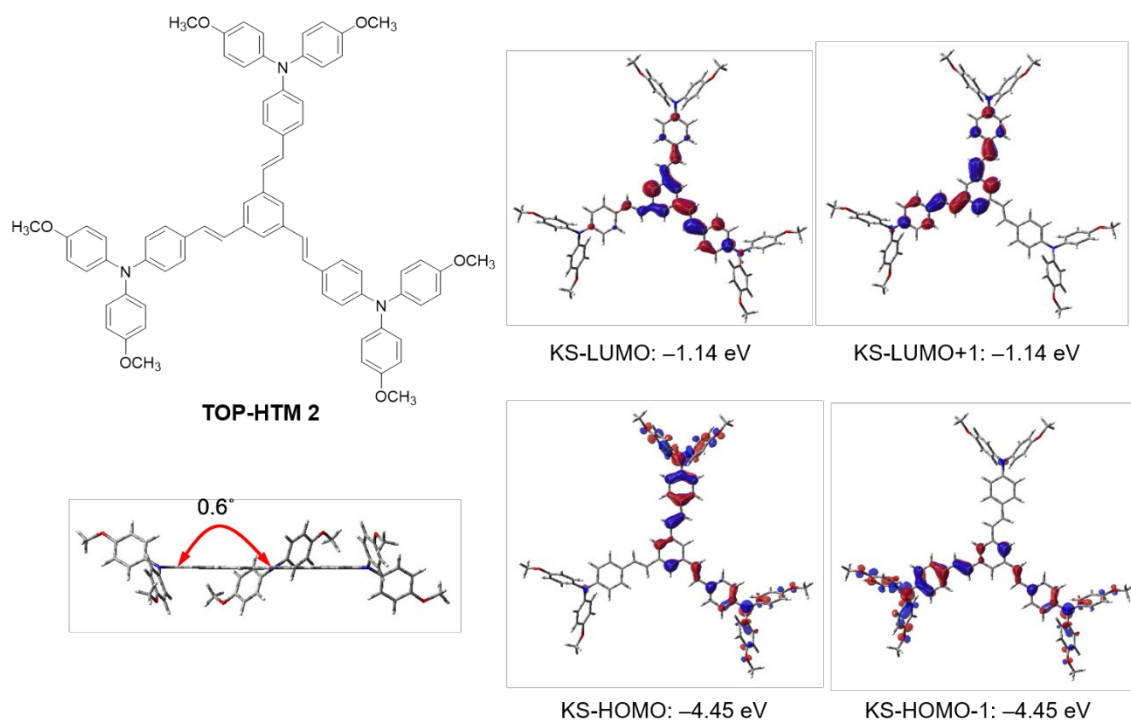


Figure S2. Optimized molecular geometries determined at the B3LYP/6-31G(d) level of theory and pictorial presentation of the frontier orbitals, a plot of the Kohn-Sham HOMO-1, HOMO, LUMO and LUMO+1 energy levels for TOP-HTM 2.

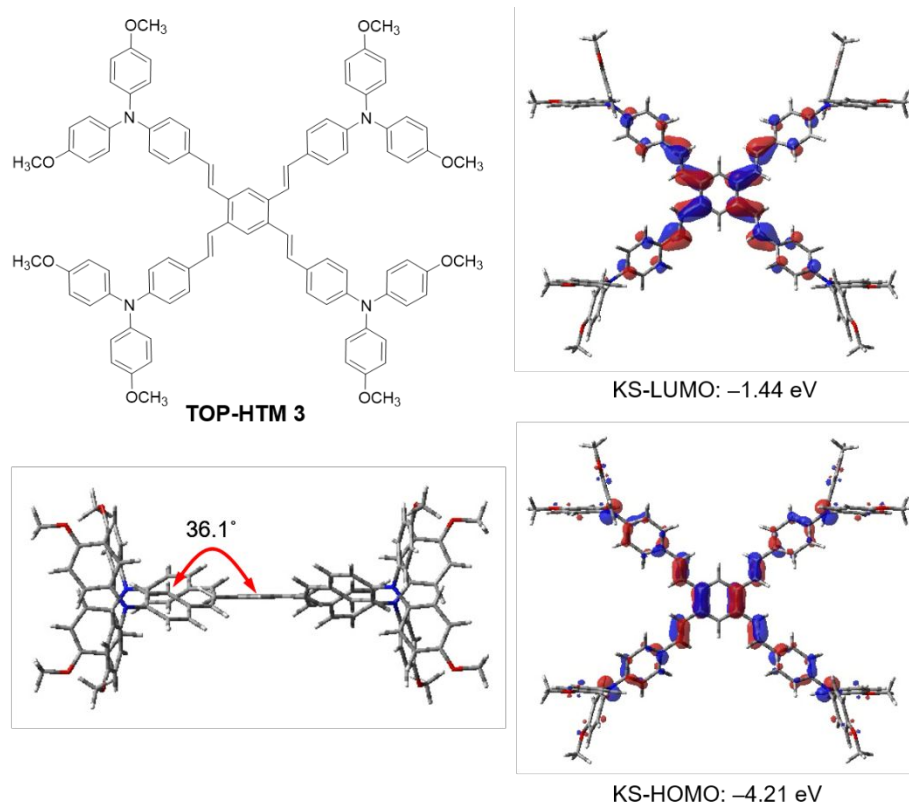


Figure S3. Optimized molecular geometries determined at the B3LYP/6-31G(d) level of theory and pictorial presentation of the frontier orbitals, a plot of the Kohn-Sham HOMO and LUMO and energy levels for TOP-HTM 3.

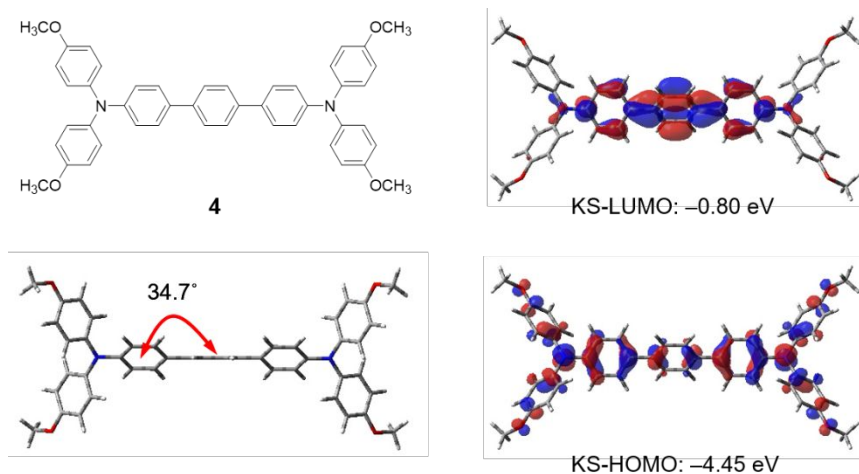


Figure S4. Optimized molecular geometries determined at the B3LYP/6-31G(d) level of theory and pictorial presentation of the frontier orbitals, a plot of the Kohn-Sham HOMO and LUMO and energy levels for 4.

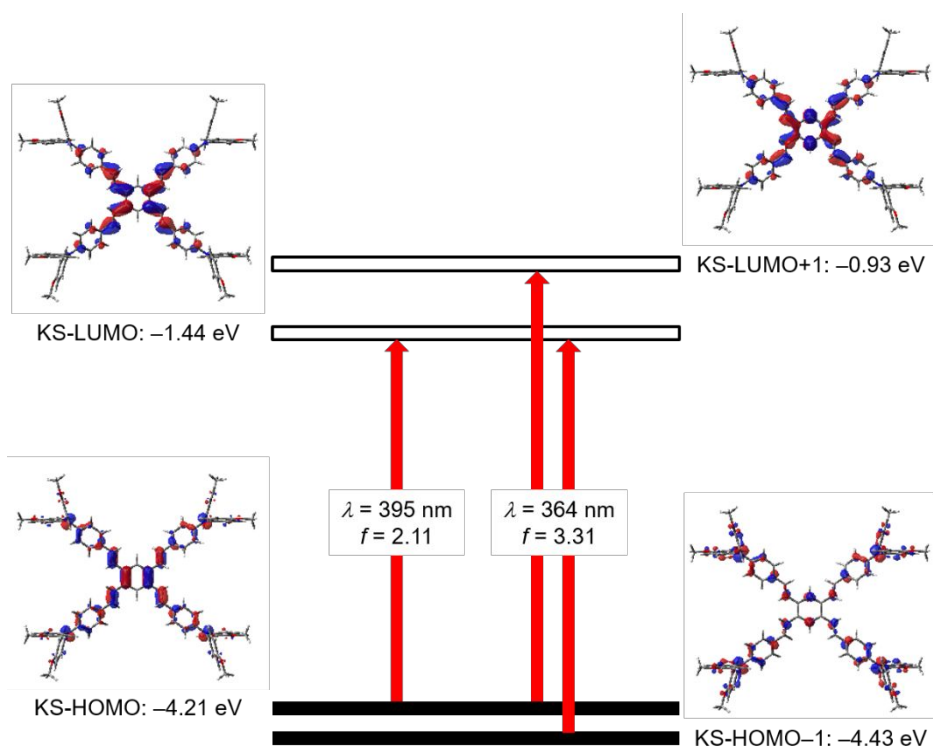


Figure S5. Comparison of the theoretical transition energies and oscillator strengths and the individual contributions to the absorption of TOP-HTM **3** obtained from TD-DFT calculations at the CAM-B3LYP/6-31G(d)//B3LYP/6-31G(d) level of theory.

Cyclic voltammograms

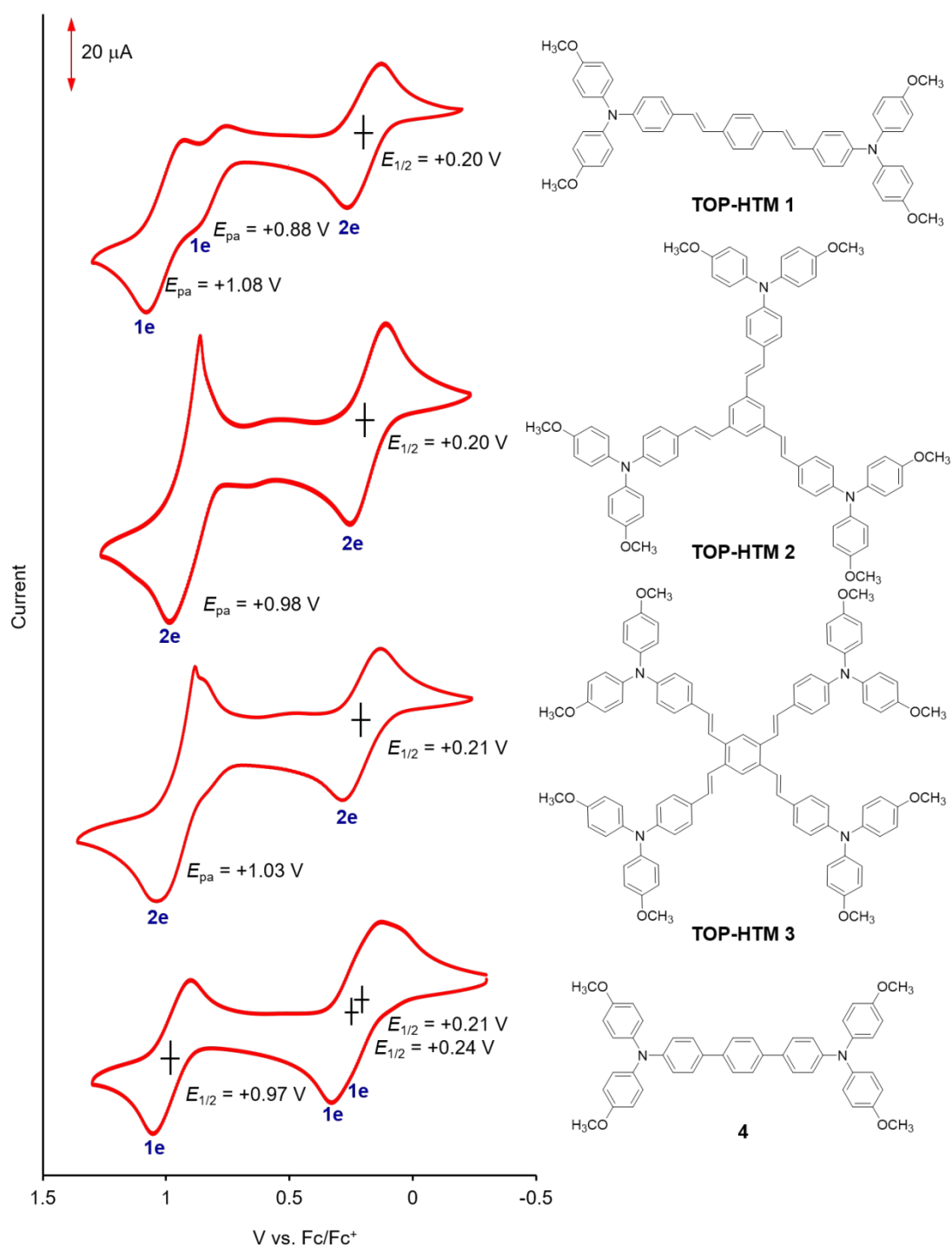


Figure S6. Cyclic voltammograms of HTMs in CH_2Cl_2 (1 mM), measured with $(n\text{-Bu})_4\text{N}^+\text{PF}_6^-$ as a supporting electrolyte at a scan rate of 100 mV/s.

Photophysical properties

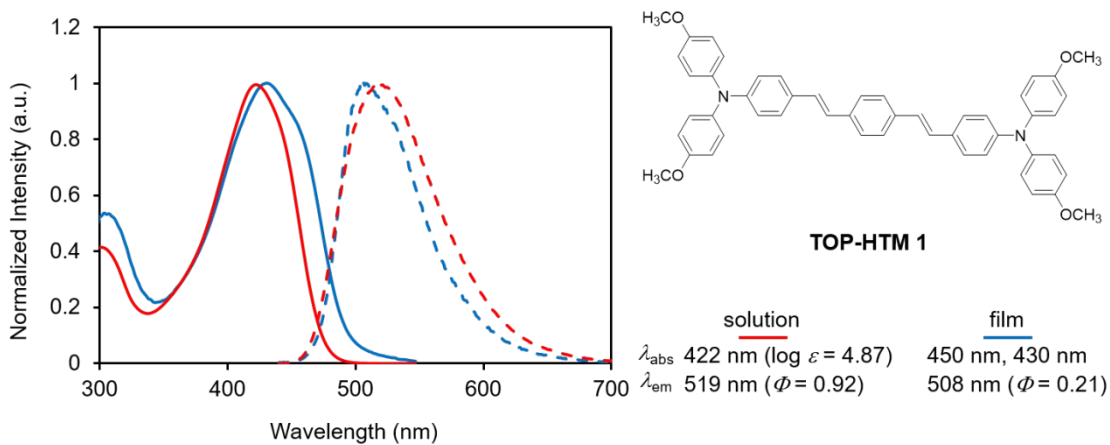


Figure S7. UV-vis absorption (solid) and fluorescence (dashed) spectra for TOP-HTM 1 in CH_2Cl_2 solution (red) and in spin-coated film (blue).

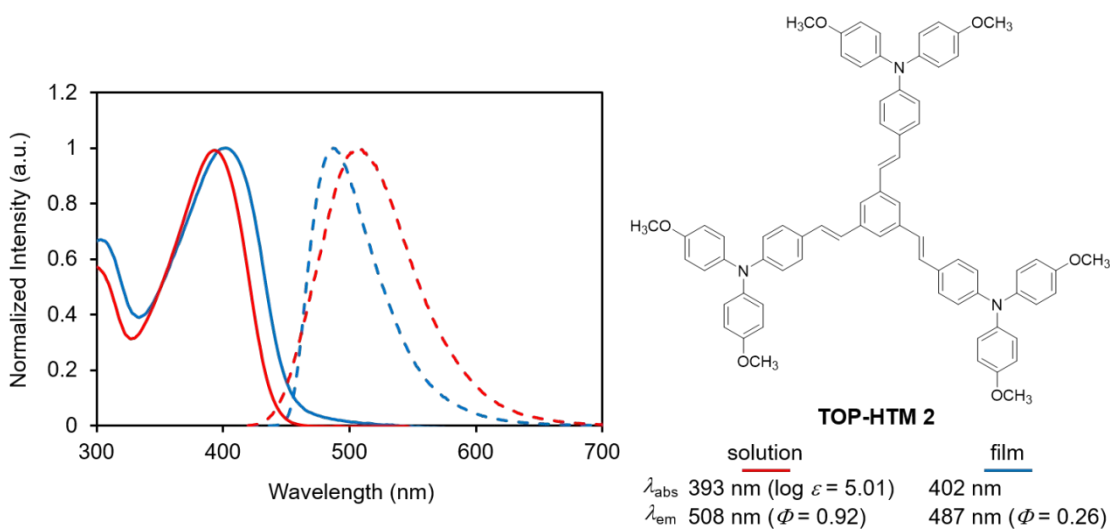


Figure S8. UV-vis absorption (solid) and fluorescence (dashed) spectra for TOP-HTM 2 in CH_2Cl_2 solution (red) and in spin-coated film (blue).

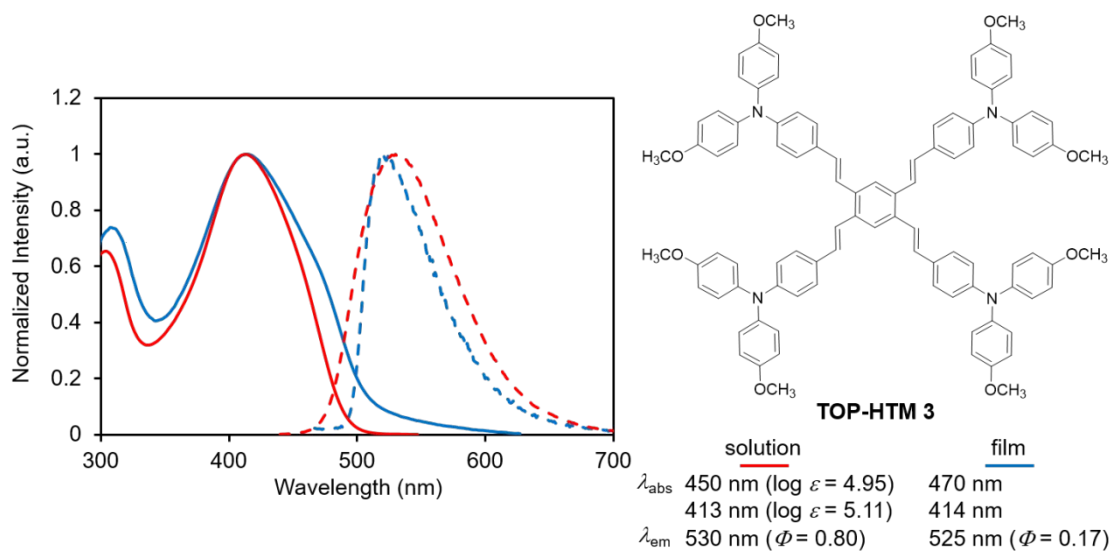


Figure S9. UV-vis absorption (solid) and fluorescence (dashed) spectra for TOP-HTM **3** in CH_2Cl_2 solution (red) and in spin-coated film (blue).

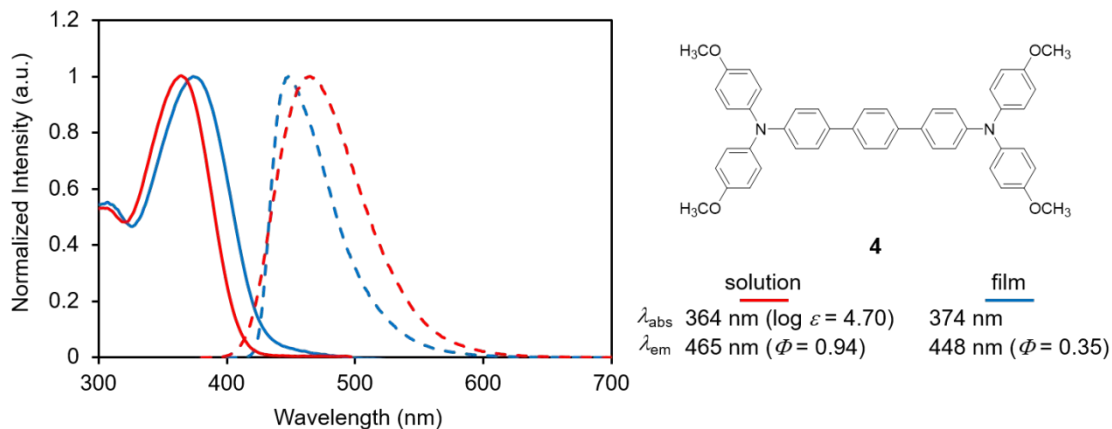


Figure S10. UV-vis absorption (solid) and fluorescence (dashed) spectra for **4** in CH_2Cl_2 solution (red) and in spin-coated film (blue).

Ionization potentials

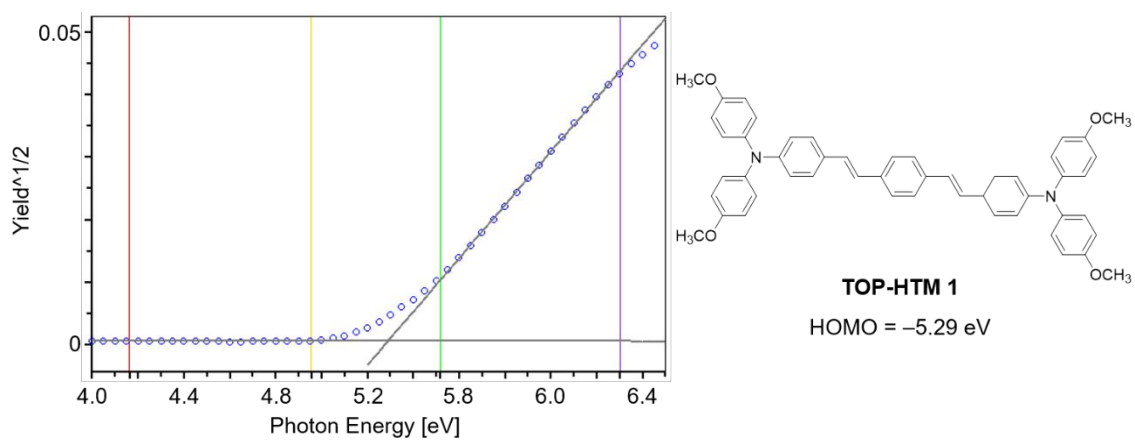


Figure S11. Photoelectron yield spectrum measured for the spin-coated film of TOP-HTM 1 under vacuum.

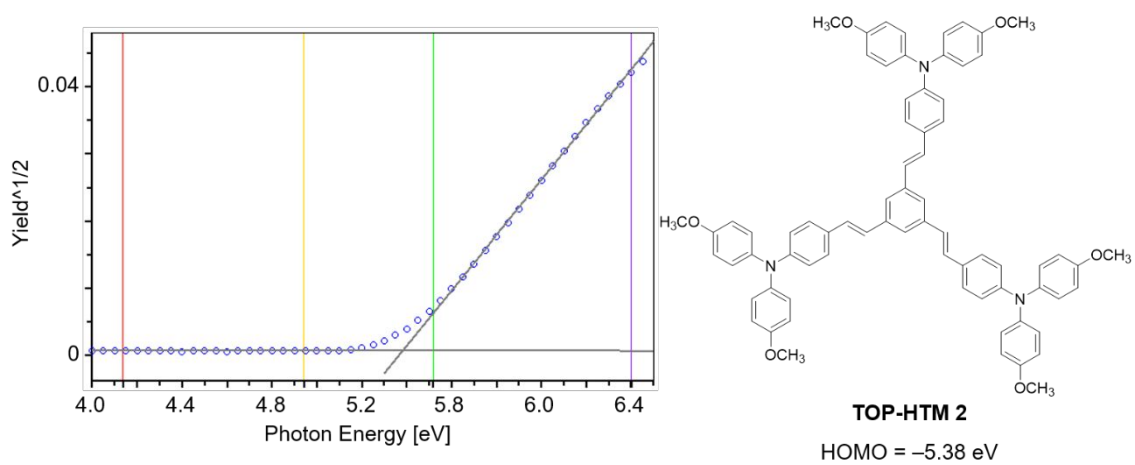


Figure S12. Photoelectron yield spectra measured for the spin-coated film of TOP-HTM 2 under vacuum.

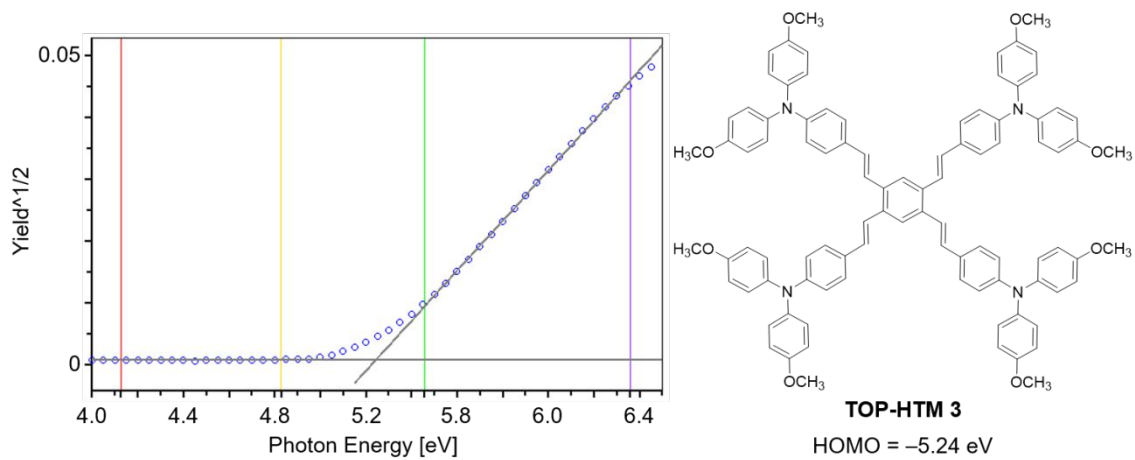


Figure S13. Photoelectron yield spectra measured for the spin-coated film of TOP-HTM **3** under vacuum.

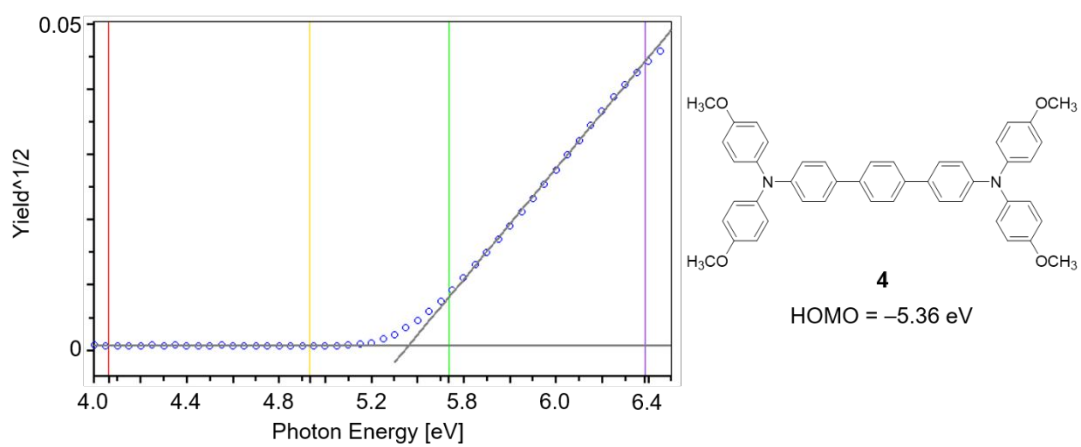


Figure S14. Photoelectron yield spectra measured for the spin-coated film of Reference **4** under vacuum.

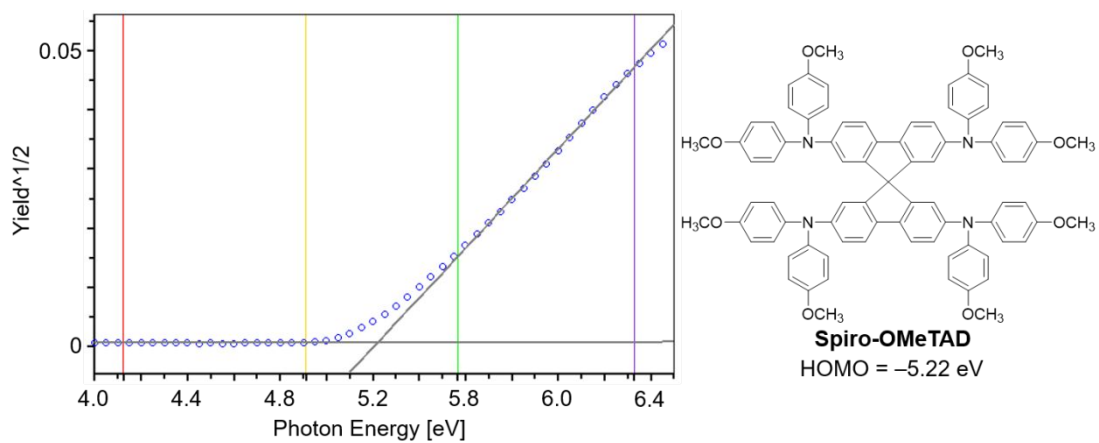


Figure S15. Photoelectron yield spectra measured for the spin-coated film of Spiro-OMeTAD under vacuum.

Thermal properties

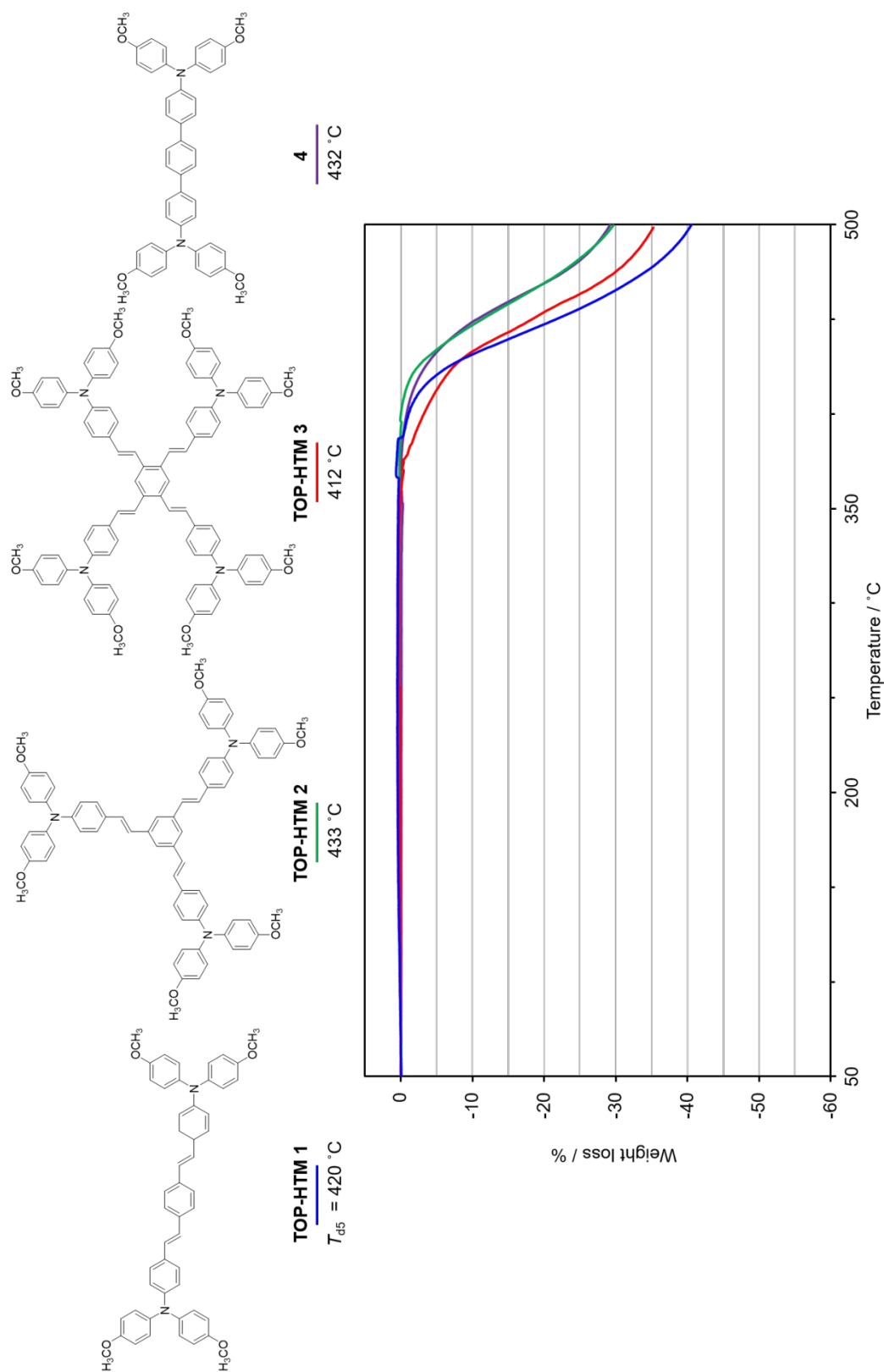


Figure S16. Thermogravimetric analyses of HTMs heating at 10 °C/min under N₂.

Glass transition temperatures (T_g) for additive-free X-shaped TOP-HTM **3** and Spiro-OMeTAD were measured by differential scanning calorimetry (DSC) method. The T_g of TOP-HTM **3** was detected at 120 °C (Figure S16a) a high value comparable to that of Spiro-OMeTAD (122 °C) (Figure S17a).

The T_g of Spiro-OMeTAD and TOP-HTM **3** with additives were also measured. HTMs were dissolved in chlorobenzene (PhCl, 1 mL) at concentration of 40 mg with the addition of LiTFSI (6.0 mg) and TBP (19.0 μ L) at 85 °C. After filtration of the solution, the filtrate was evaporated under reduced pressure and dried at 70 °C under N₂ atmosphere for 30 min. Whereas T_g of Spiro-OMeTAD was decreased to 96 °C (Figure S17b), TOP-HTM **3** retained higher value of 105 °C, suggesting the amorphous phase of TOP-HTM **3** should be more resistance to the presence of LiTFSI than Spiro-OMeTAD.

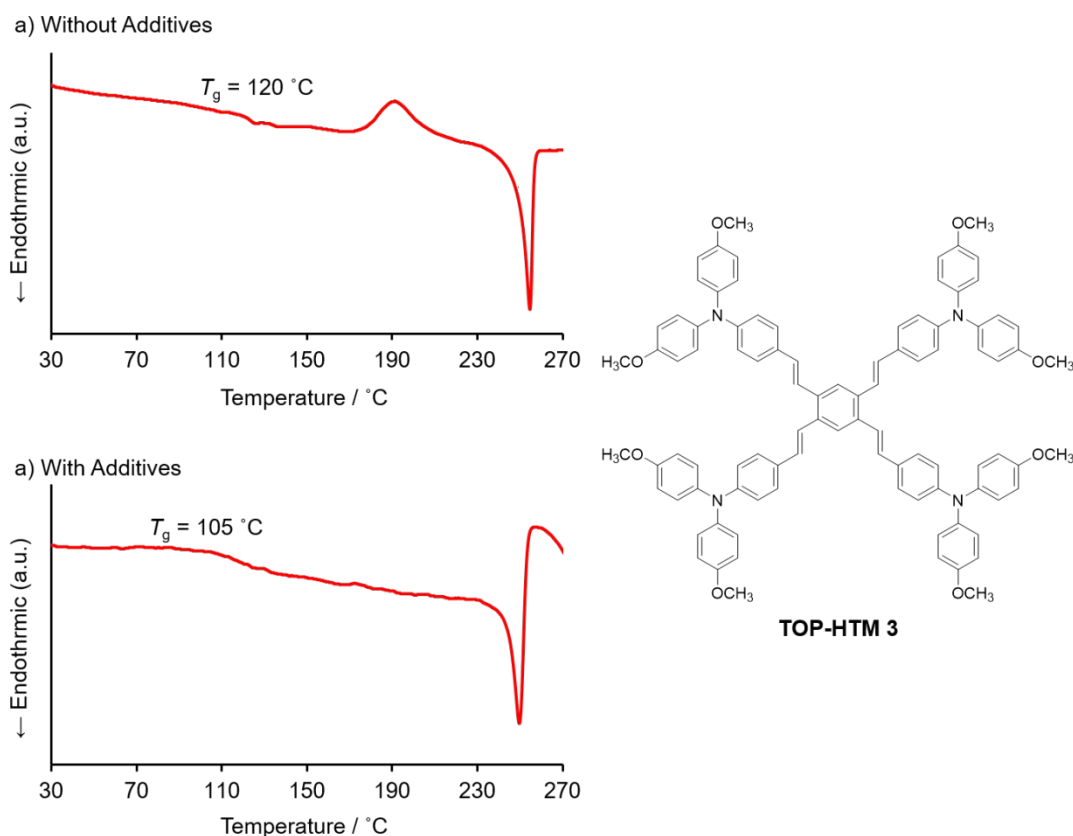


Figure S17. Differential scanning calorimetry of TOP-HTM **3** (a) without and (b) with additives heating at 10 °C/min under N₂.

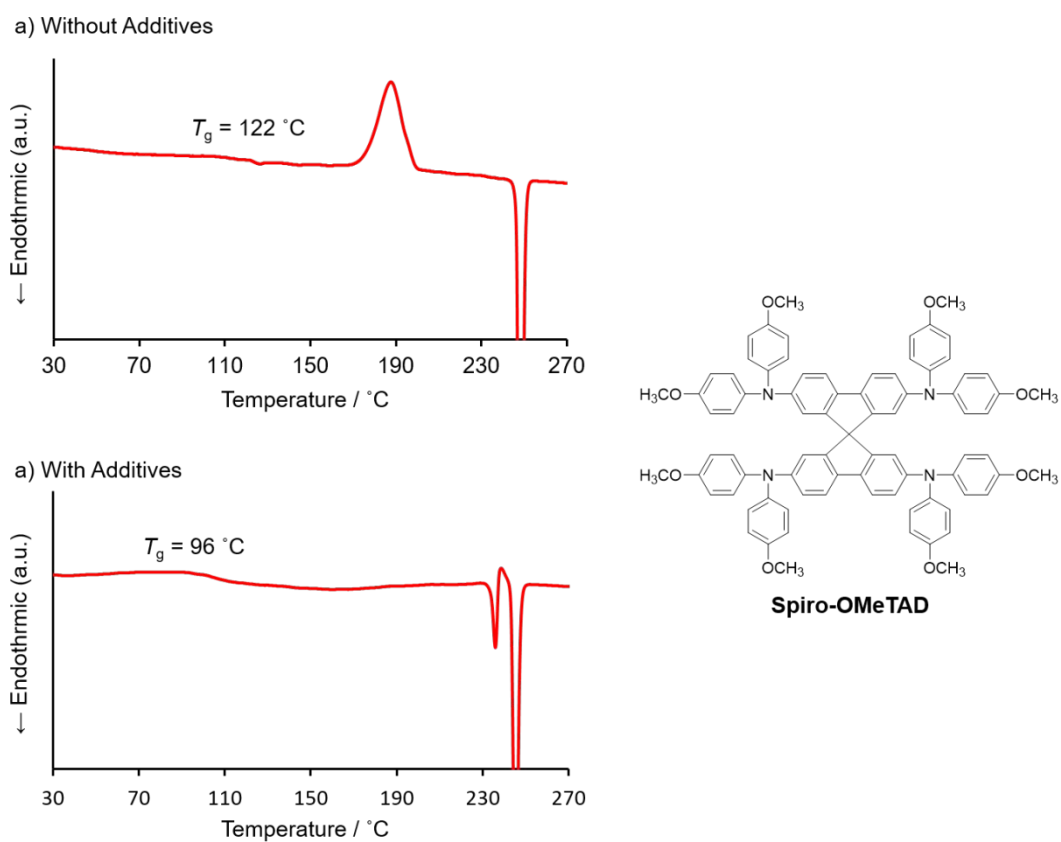


Figure S18. Differential scanning calorimetry of Spiro-OMeTAD (a) without and (b) with additives heating at 10 °C/min under N₂.

Estimation of hole mobilities and conductivities

The hole mobilities and the conductivities in the films of HTMs were measured for hole-only devices. The devices were fabricated in a structure of ITO / PEDOT:PSS (45 nm) / HTMs (150–250 nm) / Au (80 nm). The ITO-coated glass substrate (5 Ω /sq, 2.5 cm \times 2.5 cm, GEOMATEC) was washed carefully under ultrasonic irradiation using acetone (15 min), and ethanol (15 min). The substrate was subjected to O₃/ultraviolet treatment with a Filgen UV230 for 15 min. A thin layer of PEDOT:PSS (Nagase ChemteX, Denatron PT-100) was prepared onto the ITO surface by the spin-coating (5000 rpm, 60 s). The resulting substrate was heated at 200 °C for 10 min under ambient conditions. Then, hole transporting layer was prepared onto PEDOT:PSS layer by spin-coating (slope 5 s, 2000 rpm, 40 s, slope 5 s) of 1,1,2,2-tetrachloroethane solution of new HTMs or chlorobenzene solution of Spiro-OMeTAD with a concentration of 70 mg/mL. The film thicknesses were measured with Alpha-Step IQ (KLA-Tencor Co.). As a counter electrode, Au was deposited on the hole transporting layer by vacuum evaporation. The current density–voltage curves of the devices were taken with a Keithley 2400 source.

The hole mobilities were measured from the space-charge-limited of current (SCLC) region of J – V characteristics (Figure S19) obtained in the dark calculated using the Mott-Gurney law by fitting Equation 1, where J is the current density, ϵ_0 is the permittivity of free space (8.85×10^{-12} F/m), ϵ is the relative permittivity of the material (approaching 3 for organic semiconductors), μ is the hole mobility, V is the applied voltage, and d is the thickness of the active layer, respectively.

$$J = \frac{9}{8} \epsilon \epsilon_0 \mu \frac{V^2}{d^3} \quad 1$$

The conductivities were estimated from the Ohmic region of the low voltage of J – V characteristics obtained in the dark using the Ohm's law by fitting Equation 2, where σ is the conductivity, J is the current density, d is the thickness of the active layer and V is the applied voltage, respectively.

$$\sigma = \frac{J \cdot d}{V} \quad 2$$

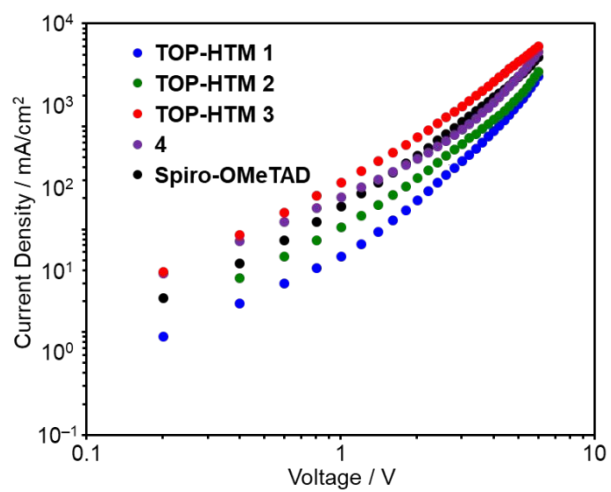


Figure S19. J - V characteristics of hole-only devices for HTMs.

Steady-state and time-resolved photoluminescence measurements

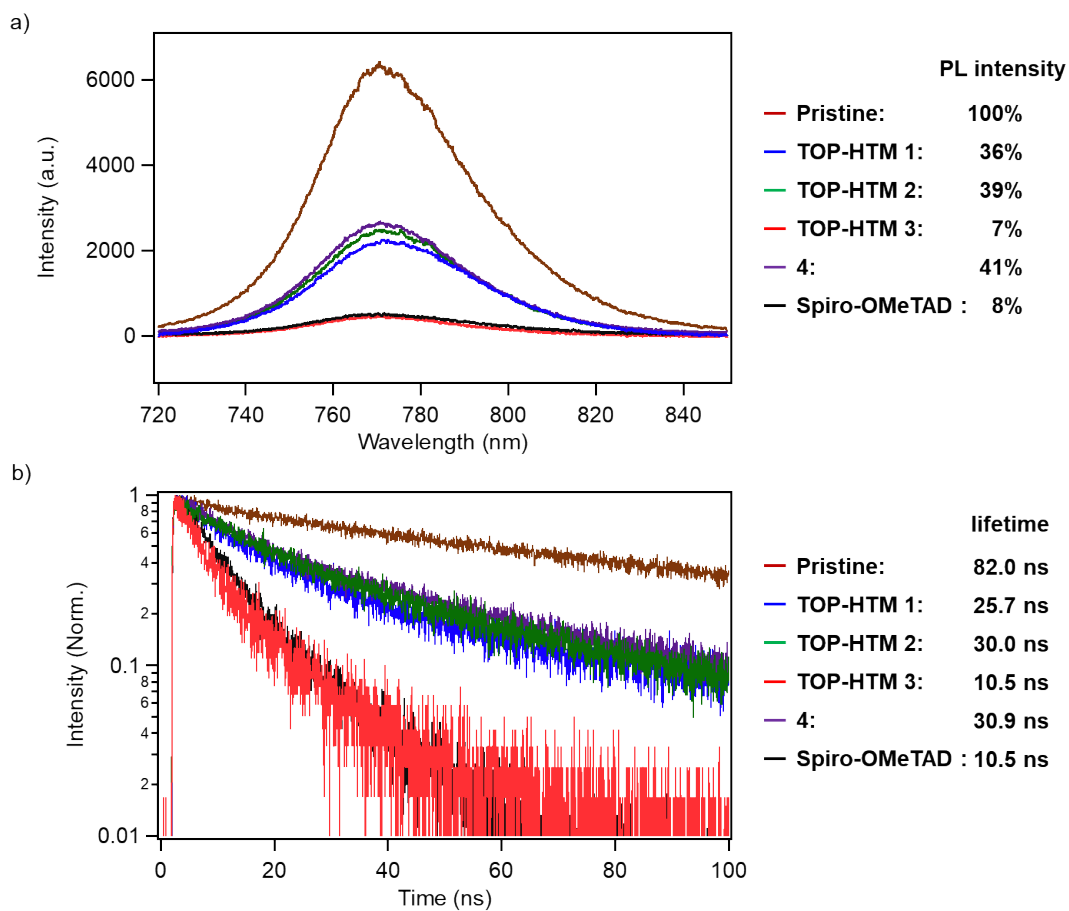


Figure S20. (a) Steady-state and (b) time-resolved PL spectra of the pristine perovskite and perovskite/additive-containing HTM films excited at 688 nm with excitation fluence of 127 nJ cm^{-2} .

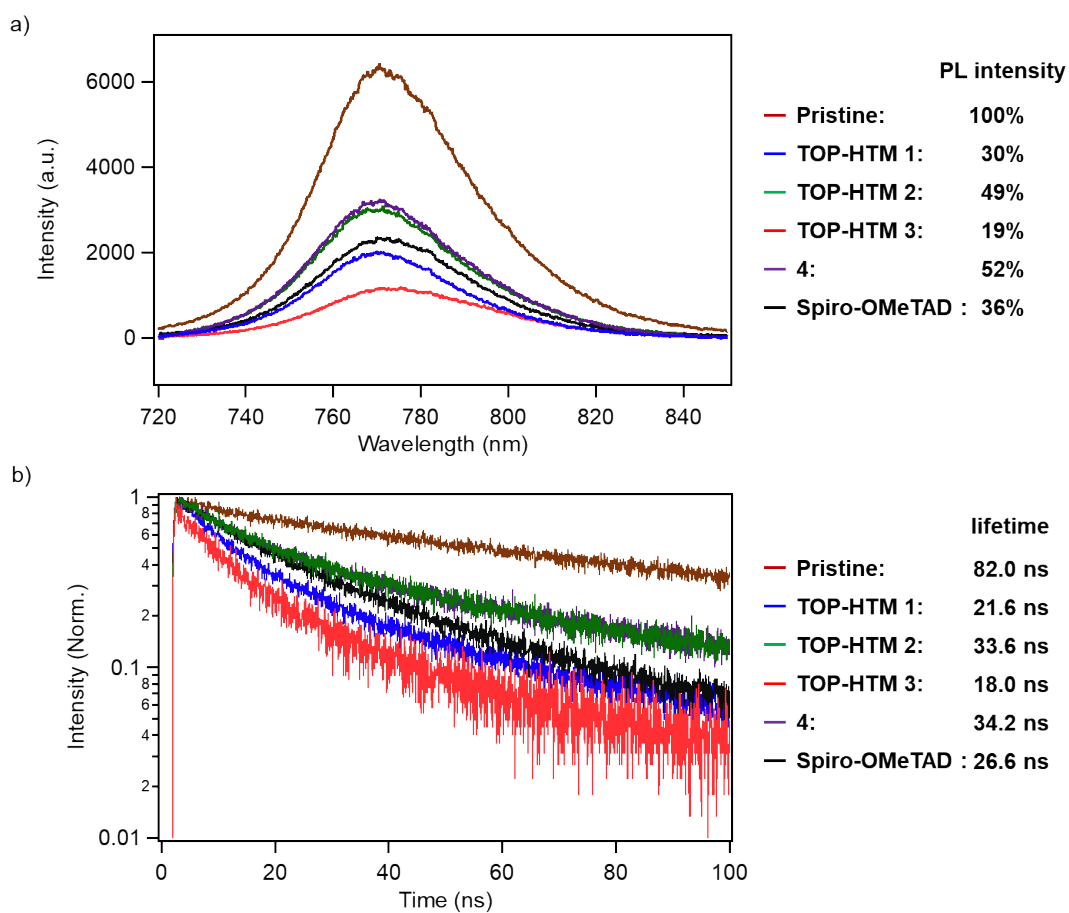


Figure S21. (a) Steady-state and (b) time-resolved PL spectra of the pristine perovskite and perovskite/additive-free HTM films excited at 688 nm with excitation fluence of 127 nJ cm^{-2} .

Preparation of perovskite solar cells

Preparation of TiO₂ layer

Patterned transparent conducting oxide substrate (FTO, 25 mm × 25 mm, Asahi Glass Co., Ltd., Japan) was treated with ultrasonic cleaning for 10 min with a 1 wt% neutral aqueous detergent solution, acetone, 2-propanol, and distilled water, respectively, and then subjected to O₃/ultraviolet treatment for 15 min. FTO substrate was covered with a compact TiO₂ layer by spray pyrolysis of ethanol solution (0.05 M) of titanium diisopropoxide bis(acetylacetonate) (75wt% in 2-propanol, Tokyo Chemical Industry Co., Ltd. (TCI)) at 450 °C. The resulting compact TiO₂ layer was treated with an aqueous solution (100 mL) of TiCl₄ (440 μL, special grade, Wako Pure Chemical Industries Ltd. (Wako)) at 70 °C for 30 min, followed by rinsing with distilled water. The substrate was sintered at 500 °C for 20 min. Subsequently, mesoporous-TiO₂ layer (thickness: 100 nm; average particle size: ca. 20 nm) was deposited on the plate by spin-coating (slope 5 s, 5000 rpm, 30 s, slope 5 s) of a suspension of TiO₂ paste (PST-18NR, JGC Catalysts and Chemicals Ltd.) in ethanol (paste : ethanol = 1 : 8 wt ratio), followed by sintering at 500 °C for 30 min. The obtained substrate was treated with O₃/ultraviolet cleaning for 15 min before used for perovskite layer fabrication.

Preparation of perovskite layer²

In a glove box filled with N₂ gas, the perovskite precursor solution was prepared using CH₃NH₃PbI₃·DMF complex (TCI) and DMSO (super dehydrated, Wako). A 1.25 M solution of CH₃NH₃PbI₃ in DMSO and DMF was deposited on the mesoporous TiO₂ films by spin-coating (slope 1 s, 1000 rpm 40 s, slope 1 s, 0 rpm. 30 s, slope 5 s, 5000 rpm 20 s, slope 1 s: At the last 3 s of spin-coating, 0.5 mL of toluene was slowly dropped on the rotating substrate.). The resulting transparent film was annealed on a hot plate at 45 °C for 10 min, 55 °C for >10 min, 75 °C for 10 min, 100 °C for 30 min to form perovskite layer.

Preparation of hole transporting layer and Au electrode

Additive-free HTM solutions were prepared at concentration of 40 mg/mL in 1,1,2,2-tetrachloroethane (TCE) at 70 °C.

In additive-containing HTM-based devices, Spiro-OMeTAD (Merck) was dissolved in chlorobenzene (PhCl, 1 mL) at concentration of 73.5 mg (0.06 M) with the addition of [tris(2-(1*H*-pyrazol-1-yl)-4-*tert*-butylpyridine)cobalt(III) tris(bis(trifluoromethylsulfonyl)imide)] (FK209, 13.5 mg, 9.0 mM, Aldrich), lithium bis(trifluoromethylsulfonyl)imide (LITFSI, 9.1 mg, 0.032 mM, Wako), and 4-*tert*-butylpyridine (TBP, 28.8 μL, 0.20 mM, Aldrich) at 70 °C.³ In new HTMs, we initially prepared TCE solution. However, TCE was changed color by the addition of

additives and device performance of PSC using TCE solution was low. Therefore, chlorobenzene (PhCl) was used as solvent. HTMs were dissolved at concentration of 40 mg/mL with LiTFSI and TBP as additives. The amount of LiTFSI and TBP were 4.8 mg and 15.2 μL for TOP-HTM 1, 2.4 mg and 7.6 μL for TOP-HTM 2, 6.0 mg and 19.0 μL for TOP-HTM 3, 2.0 mg and 6.3 μL for 4, respectively. TOP-HTM 3 solution was heated at 85 °C and other HTM solutions were heated at 70 °C.

Hole transporting layers were deposited on the perovskite layer by spin-coating (slope 5 s, 4000 rpm 30 s, slope 5 s). The resulting film was dried on a hot plate at 70 °C for 30 min. Finally, a gold electrode (80 nm) was thermally deposited on the hole transporting layer.

Solar cell device performances

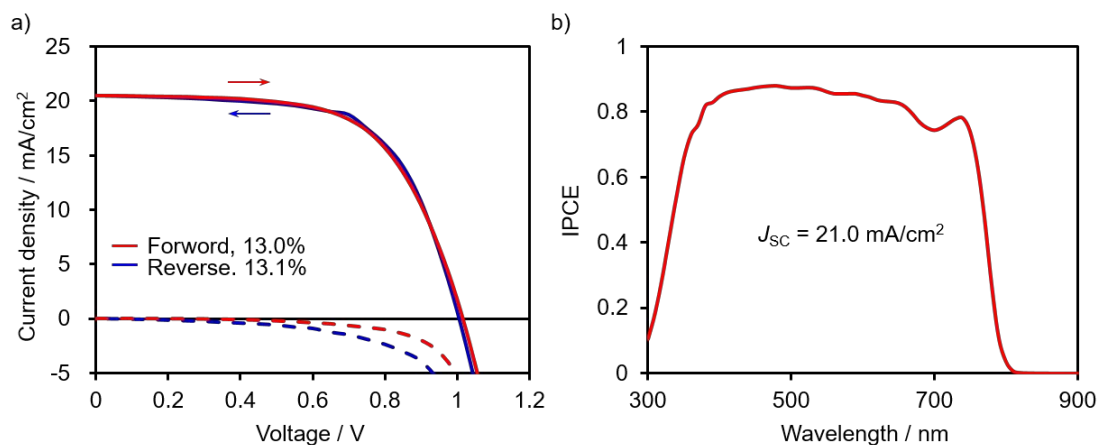


Figure S22. a) J - V characteristics measured by forward (red) and reverse (blue) scans under AM 1.5 G irradiation (100 mW/cm²) (solid line) and dark condition (dashed line) and b) IPCE spectrum and the corresponding integrated J_{SC} value of perovskite solar cell using TOP-HTM 1 with additives.

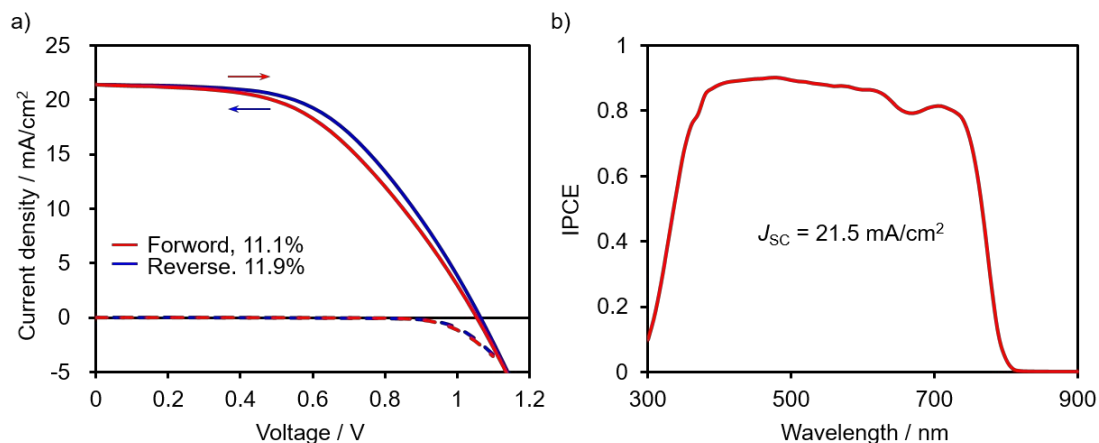


Figure S23. a) J - V characteristics measured by forward (red) and reverse (blue) scans under AM 1.5 G irradiation (100 mW/cm²) (solid line) and dark condition (dashed line) and b) IPCE spectrum and the corresponding integrated J_{SC} value of perovskite solar cell using TOP-HTM 2 with additives.

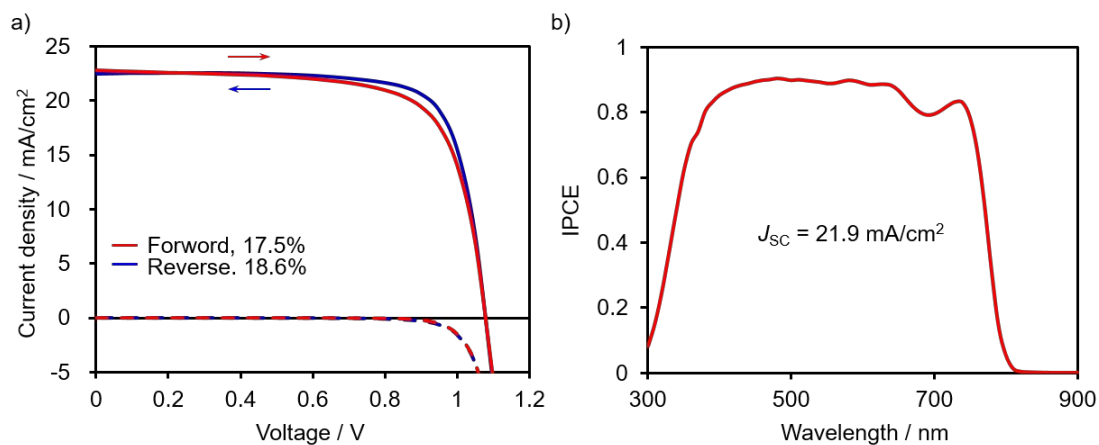


Figure S24. a) J - V characteristics measured by forward (red) and reverse (blue) scans under AM 1.5 G irradiation (100 mW/cm²) (solid line) and dark condition (dashed line) and b) IPCE spectrum and the corresponding integrated J_{SC} value of perovskite solar cell using TOP-HTM 3 with additives.

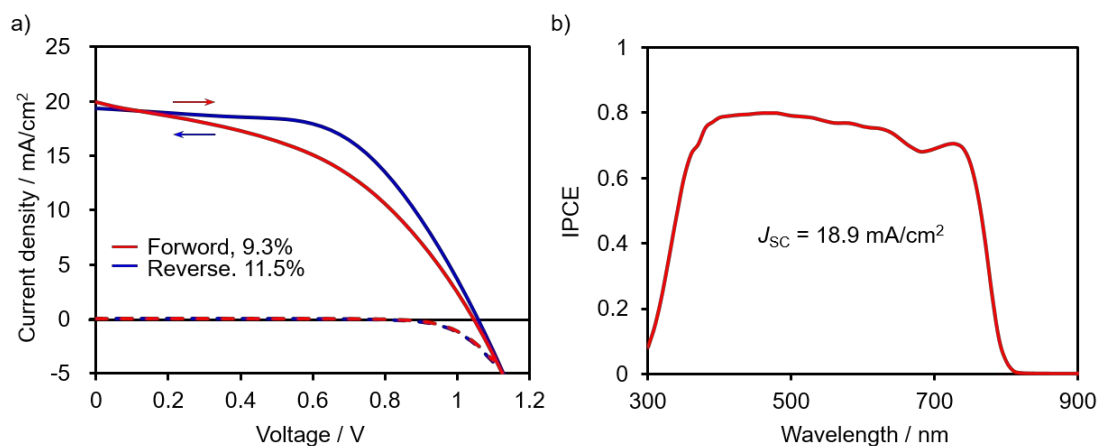


Figure S25. a) J - V characteristics measured by forward (red) and reverse (blue) scans under AM 1.5 G irradiation (100 mW/cm²) (solid line) and dark condition (dashed line) and b) IPCE spectrum and the corresponding integrated J_{SC} value of perovskite solar cell using 4 with additives.

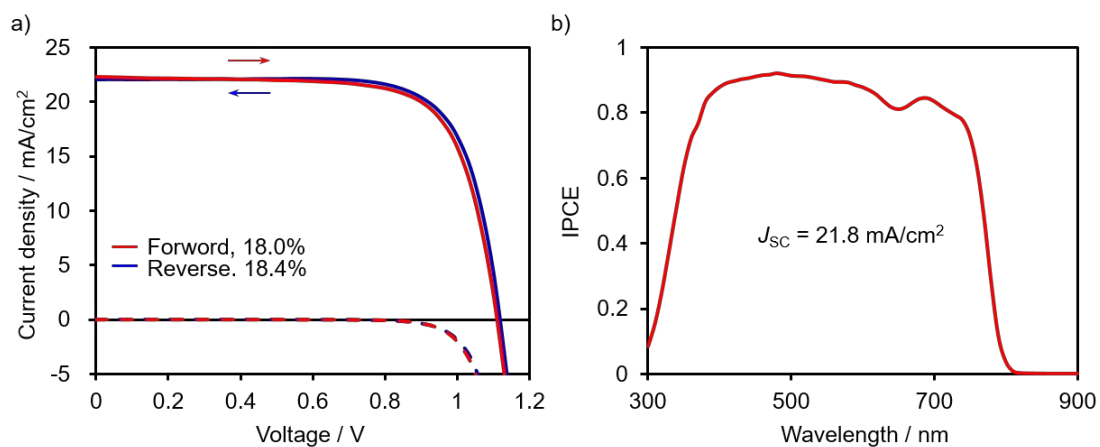


Figure S26. a) J - V characteristics measured by forward (red) and reverse (blue) scans under AM 1.5 G irradiation (100 mW/cm^2) (solid line) and dark condition (dashed line) and b) IPCE spectrum and the corresponding integrated J_{SC} value of perovskite solar cell using Spiro-OMeTAD with additives.

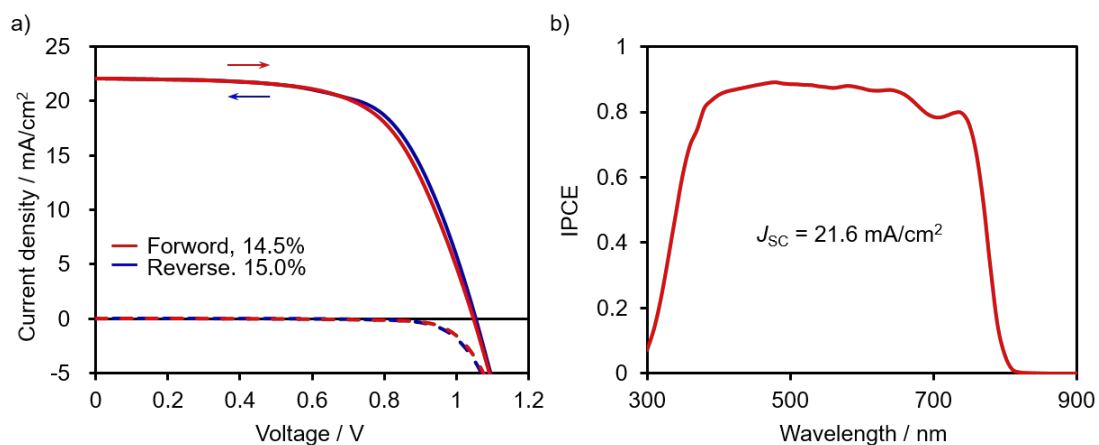


Figure S27. a) J - V characteristics measured by forward (red) and reverse (blue) scans under AM 1.5 G irradiation (100 mW/cm^2) (solid line) and dark condition (dashed line) and b) IPCE spectrum and the corresponding integrated J_{SC} value of perovskite solar cell using additive-free TOP-HTM 1.

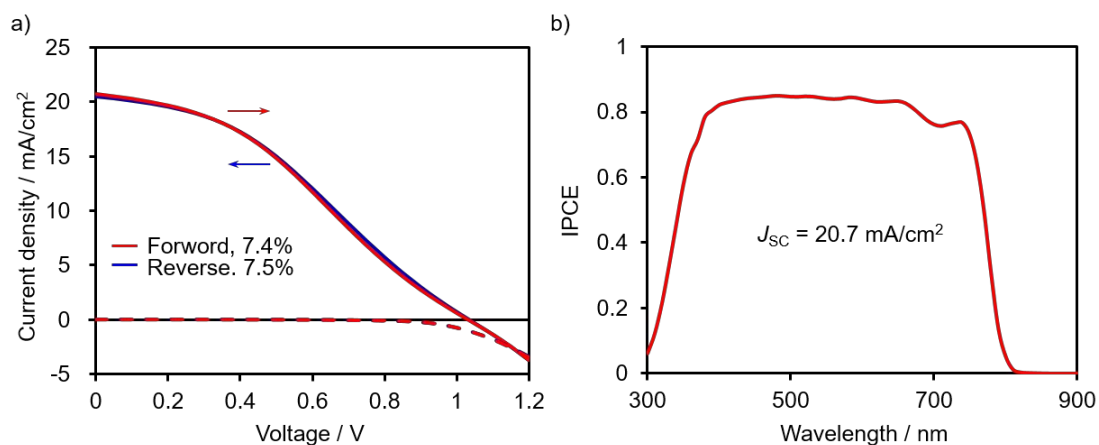


Figure S28. a) J - V characteristics measured by forward (red) and reverse (blue) scans under AM 1.5 G irradiation (100 mW/cm²) (solid line) and dark condition (dashed line) and b) IPCE spectrum and the corresponding integrated J_{SC} value of perovskite solar cell using additive-free TOP-HTM 2.

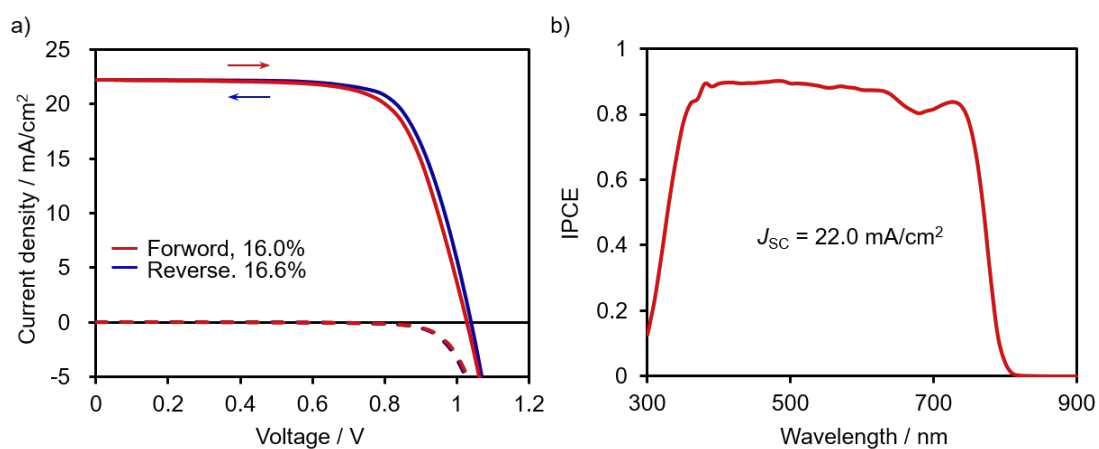


Figure S29. a) J - V characteristics measured by forward (red) and reverse (blue) scans under AM 1.5 G irradiation (100 mW/cm²) (solid line) and dark condition (dashed line) and b) IPCE spectrum and the corresponding integrated J_{SC} value of perovskite solar cell using additive-free TOP-HTM 3.

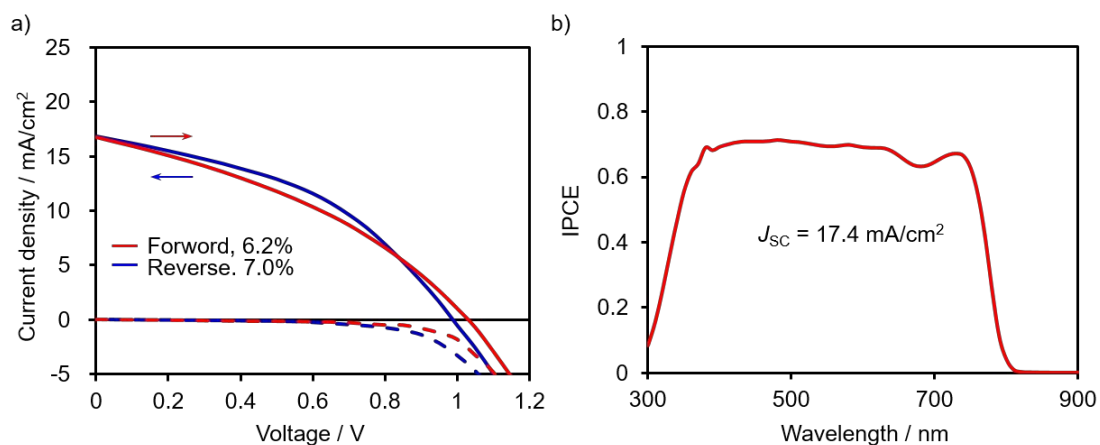


Figure S30. a) J - V characteristics measured by forward (red) and reverse (blue) scans under AM 1.5 G irradiation (100 mW/cm²) (solid line) and dark condition (dashed line) and b) IPCE spectrum and the corresponding integrated J_{SC} value of perovskite solar cell using additive-free 4.

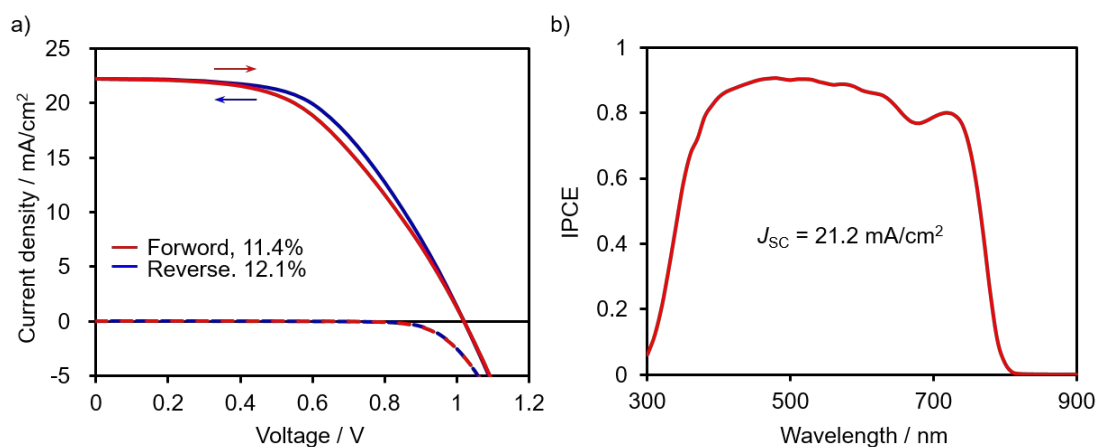


Figure S31. a) J - V characteristics measured by forward (red) and reverse (blue) scans under AM 1.5 G irradiation (100 mW/cm²) (solid line) and dark condition (dashed line) and b) IPCE spectrum and the corresponding integrated J_{SC} value of perovskite solar cell using additive-free Spiro-OMeTAD.

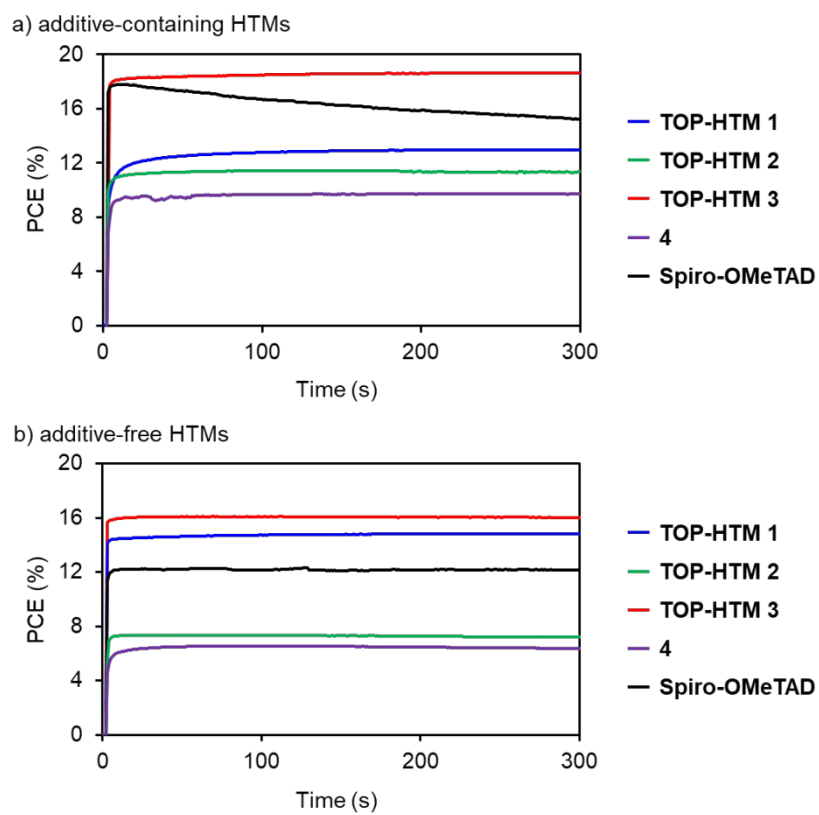


Figure S32. The stabilized power output of PSCs based on (a) additive-containing and (b) additive-free HTMs under a fixed bias at the maximum power output.

SEM Images

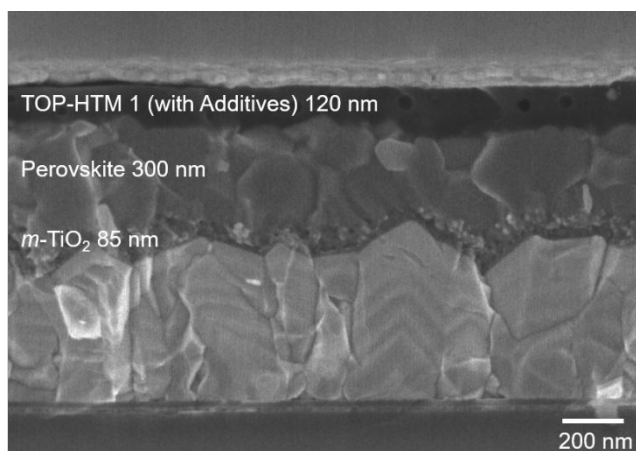


Figure S33. Cross-sectional SEM image for perovskite solar cells using TOP-HTM **1** with additives.

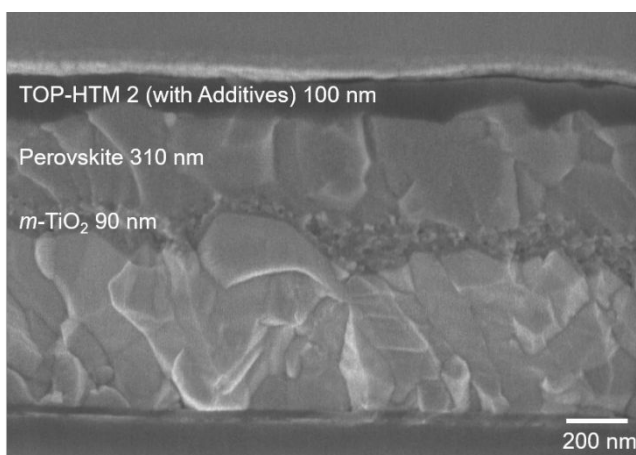


Figure S34. Cross-sectional SEM image for perovskite solar cells using TOP-HTM **2** with additives.

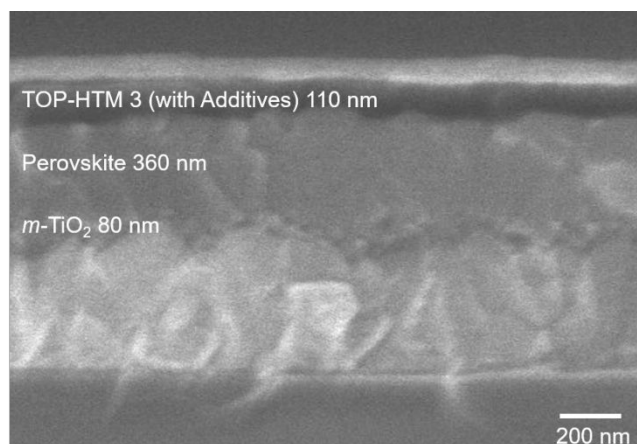


Figure S35. Cross-sectional SEM image for perovskite solar cells using TOP-HTM **3** with additives.

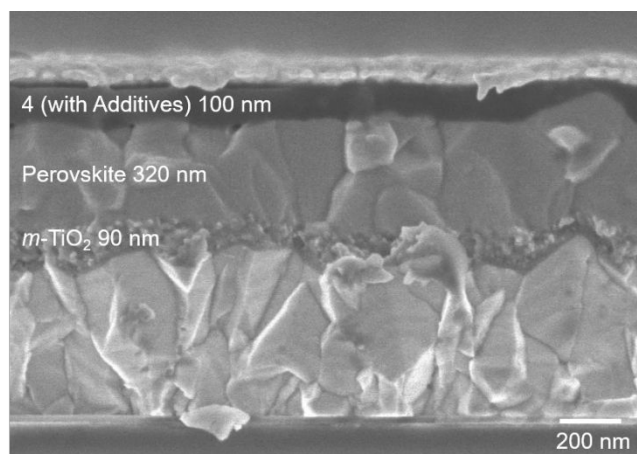


Figure S36. Cross-sectional SEM image for perovskite solar cells using **4** with additives.

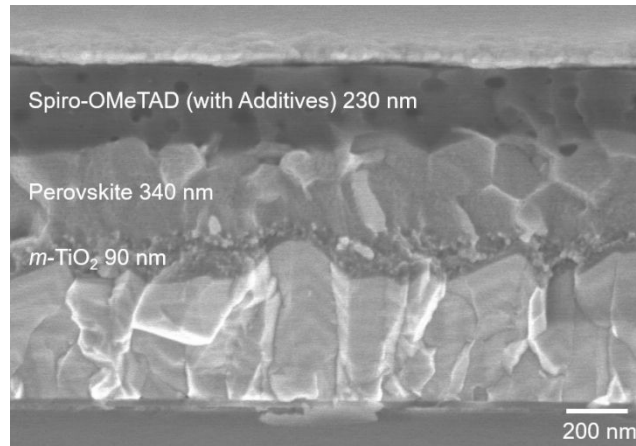


Figure S37. Cross-sectional SEM image for perovskite solar cells using Spiro-OMeTAD with additives.

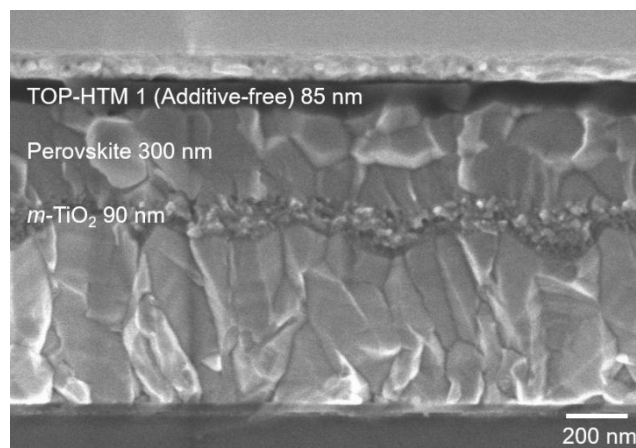


Figure S38. Cross-sectional SEM image for perovskite solar cells using additive-free TOP-HTM 1.

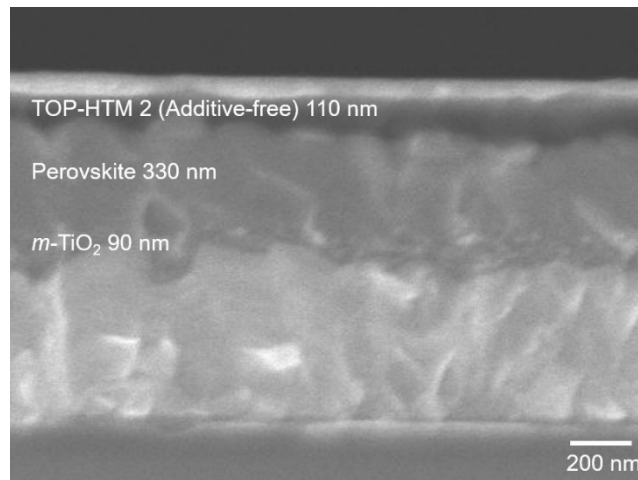


Figure S39. Cross-sectional SEM image for perovskite solar cells using additive-free TOP-HTM 2.

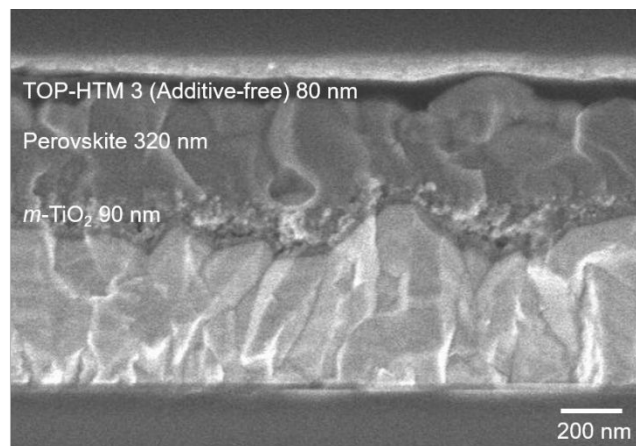


Figure S40. Cross-sectional SEM image for perovskite solar cells using additive-free TOP-HTM 3.

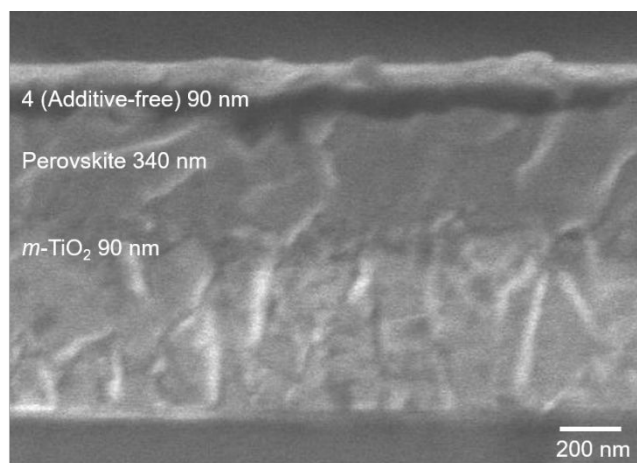


Figure S41. Cross-sectional SEM image for perovskite solar cells using additive-free 4.

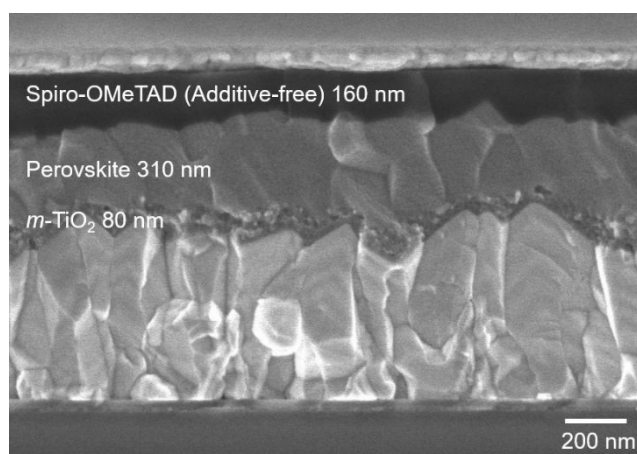


Figure S42. Cross-sectional SEM image for perovskite solar cells using additive-free Spiro-OMeTAD.

References

1. Gaussian 09, Revision C.01, Frisch, M. J.; Trucks, G. W.; Schlegel, H. B.; Scuseria, G. E.; Robb, M. A.; Cheeseman, J. R.; Scalmani, G.; Barone, V.; Mennucci, B.; Petersson, G. A.; Nakatsuji, H.; Caricato, M.; Li, X.; Hratchian, H. P.; Izmaylov, A. F.; Bloino, J.; Zheng, G.; Sonnenberg, J. L.; Hada, M.; Ehara, M.; Toyota, K.; Fukuda, R.; Hasegawa, J.; Ishida, M.; Nakajima, T.; Honda, Y.; Kitao, O.; Nakai, H.; Vreven, T.; Montgomery, J. A., Jr.; Peralta, J. E.; Ogliaro, F.; Bearpark, M.; Heyd, J. J.; Brothers, E.; Kudin, K. N.; Staroverov, V. N.; Kobayashi, R.; Normand, J.; Raghavachari, K.; Rendell, A.; Burant, J. C.; Iyengar, S. S.; Tomasi, J.; Cossi, M.; Rega, N.; Millam, J. M.; Klene, M.; Knox, J. E.; Cross, J. B.; Bakken, V.; Adamo, C.; Jaramillo, J.; Gomperts, R.; Stratmann, R. E.; Yazyev, O.; Austin, A. J.; Cammi, R.; Pomelli, C.; Ochterski, J. W.; Martin, R. L.; Morokuma, K.; Zakrzewski, V. G.; Voth, G. A.; Salvador, P.; Dannenberg, J. J.; Dapprich, S.; Daniels, A. D.; Farkas, Ö.; Foresman, J. B.; Ortiz, J. V.; Cioslowski, J.; Fox, D. J. Gaussian, Inc., Wallingford CT, 2016.
2. Ozaki, M.; Shimazaki, A.; Jung, M.; Nakaike, Y.; Maruyama, N.; Yakumar, S.; Rafieh A. I.; Sasamori, T.; Tokitoh, N.; Ekanayake, P.; Murata, M.; Murdey, R.; Wakamiya, A. A Purified, Solvent-Intercalated Precursor Complex for Wide Process Window Fabrication of Efficient Perovskite Solar Cells and Modules. *Angew. Chem., Int. Ed.* **2019**, *58*, 9389–9393.
3. Truong, M. A.; Lee, J.; Nakamura, T.; Seo, J.-Y.; Jung, M.; Ozaki, M.; Shimazaki, A.; Shioya, N.; Hasegawa, T.; Murata, Y.; Zakeeruddin, S. M.; Grätzel, M.; Murdey, R.; Wakamiya, A. Influence of Alkoxy Chain Length on the Properties of Two-Dimensionally Expanded Azulene-Core-Based Hole-Transporting Materials for Efficient Perovskite Solar Cells. *Chem.–Eur. J.* **2019**, *25*, 6741–6752.

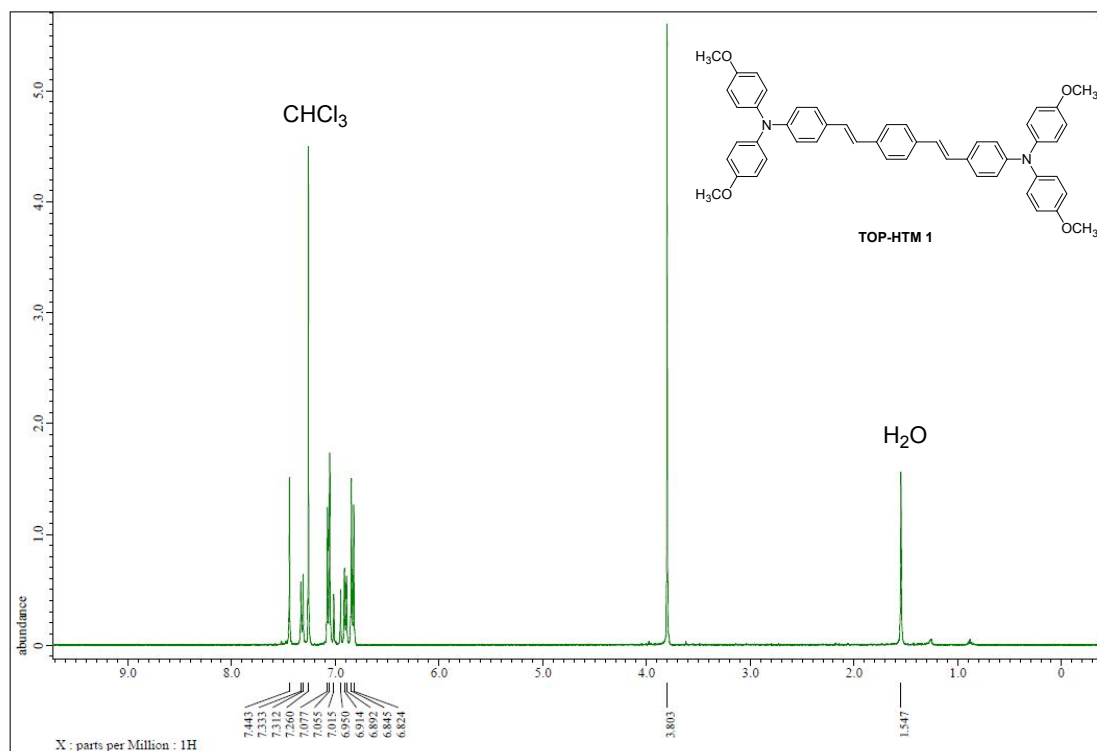


Figure S43. ^1H NMR of TOP-HTM 1 in CDCl_3 .

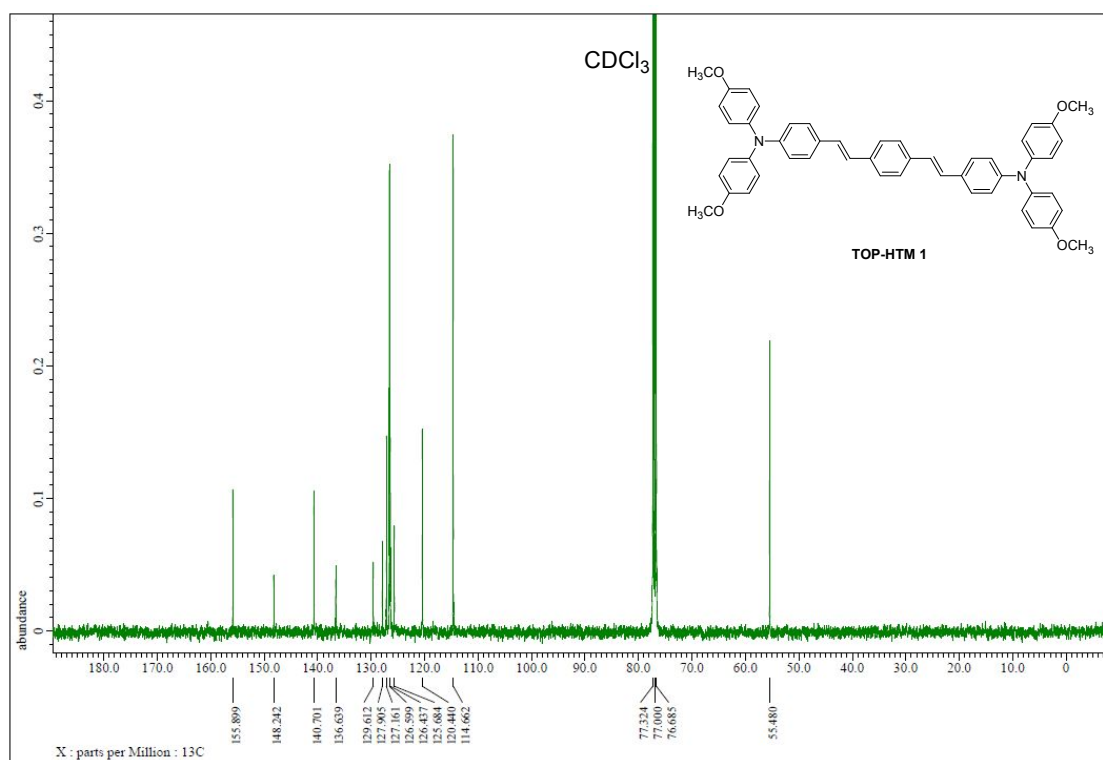


Figure S44. ^{13}C NMR of TOP-HTM 1 in CDCl_3 .

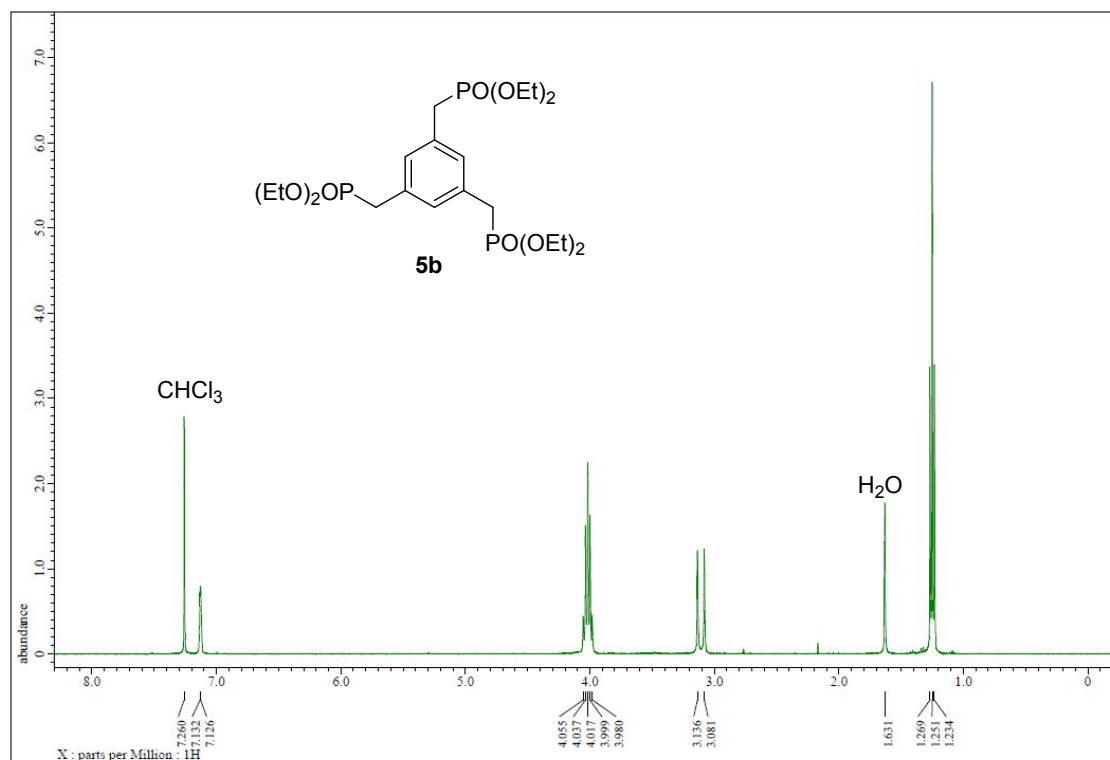


Figure S45. ¹H NMR of **5b** in CDCl₃.

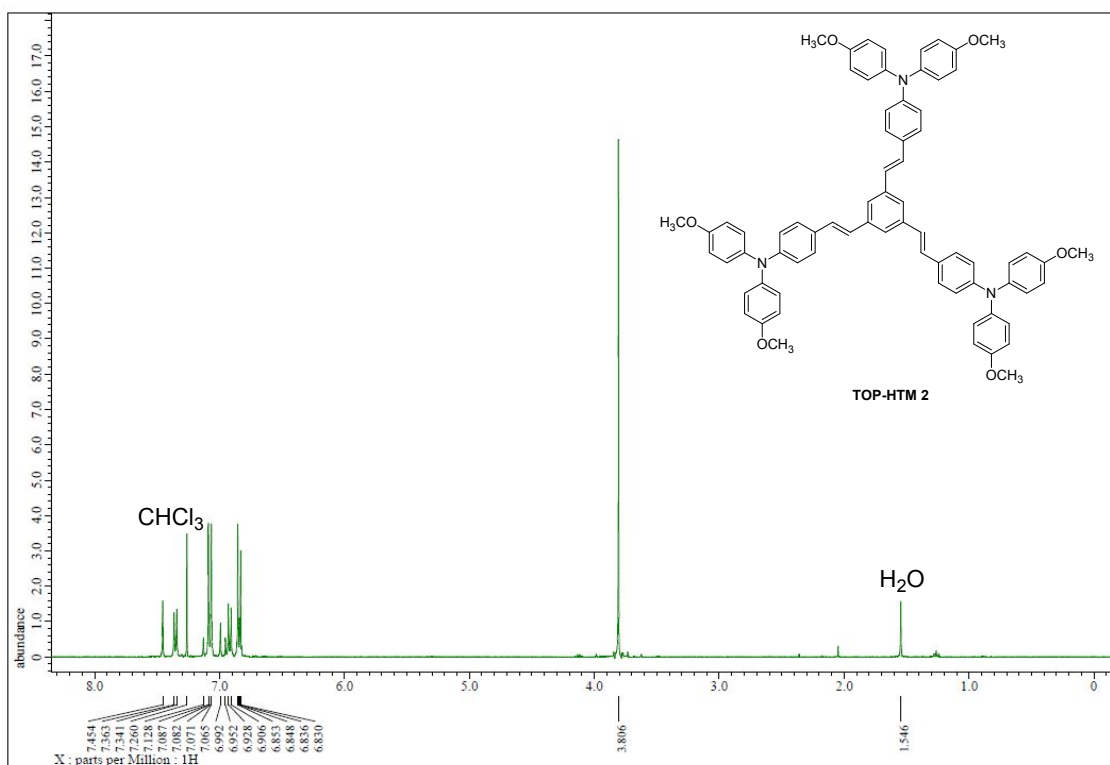


Figure S46. ¹H NMR of **TOP-HTM 2** in CDCl₃.

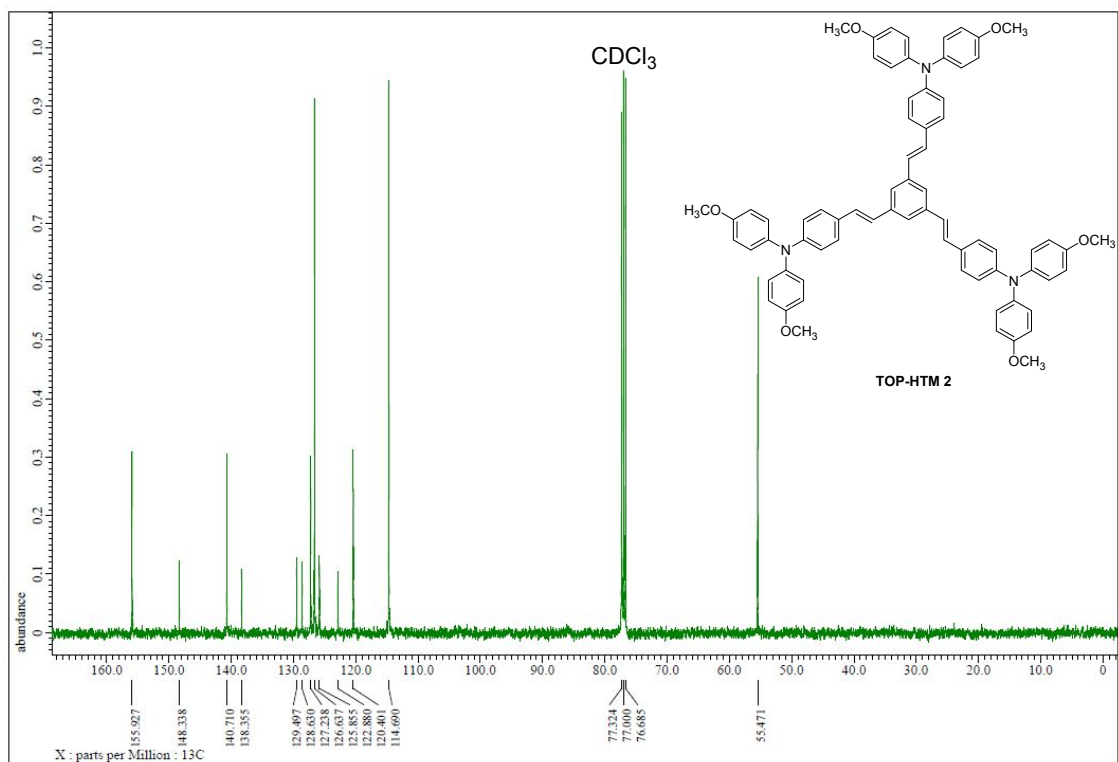


Figure S47. ¹³C NMR of TOP-HTM 2 in CDCl₃.

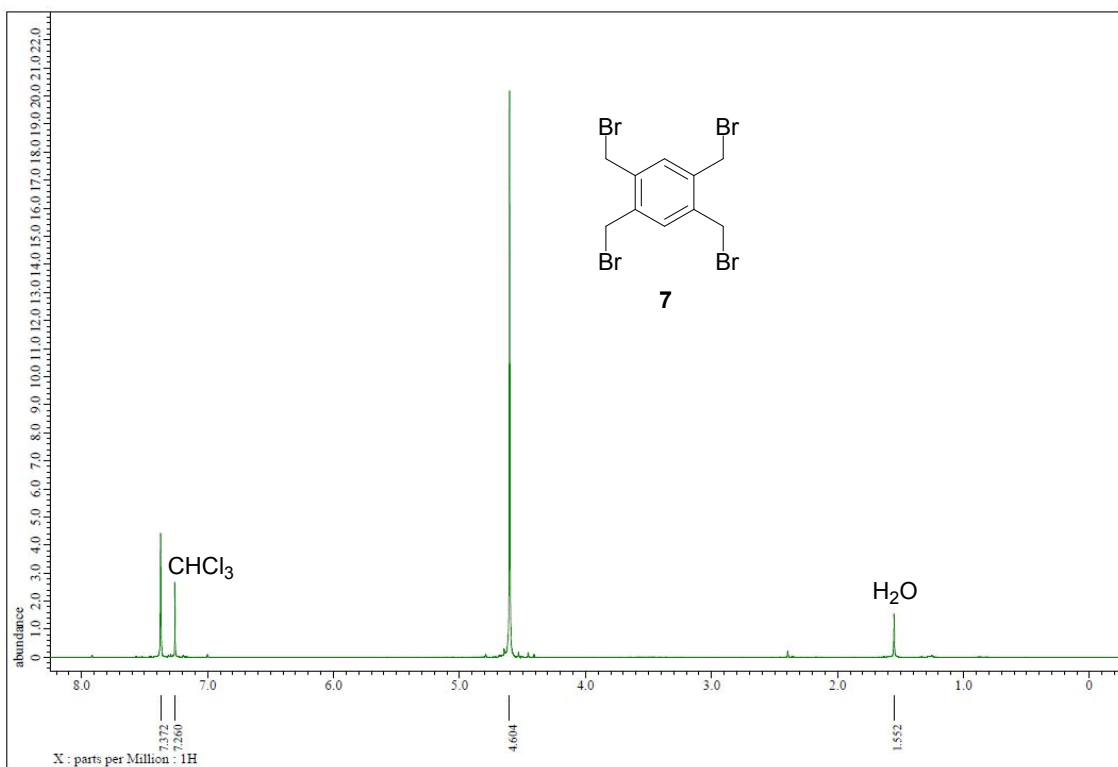


Figure S48. ¹H NMR of 7 in CDCl₃.

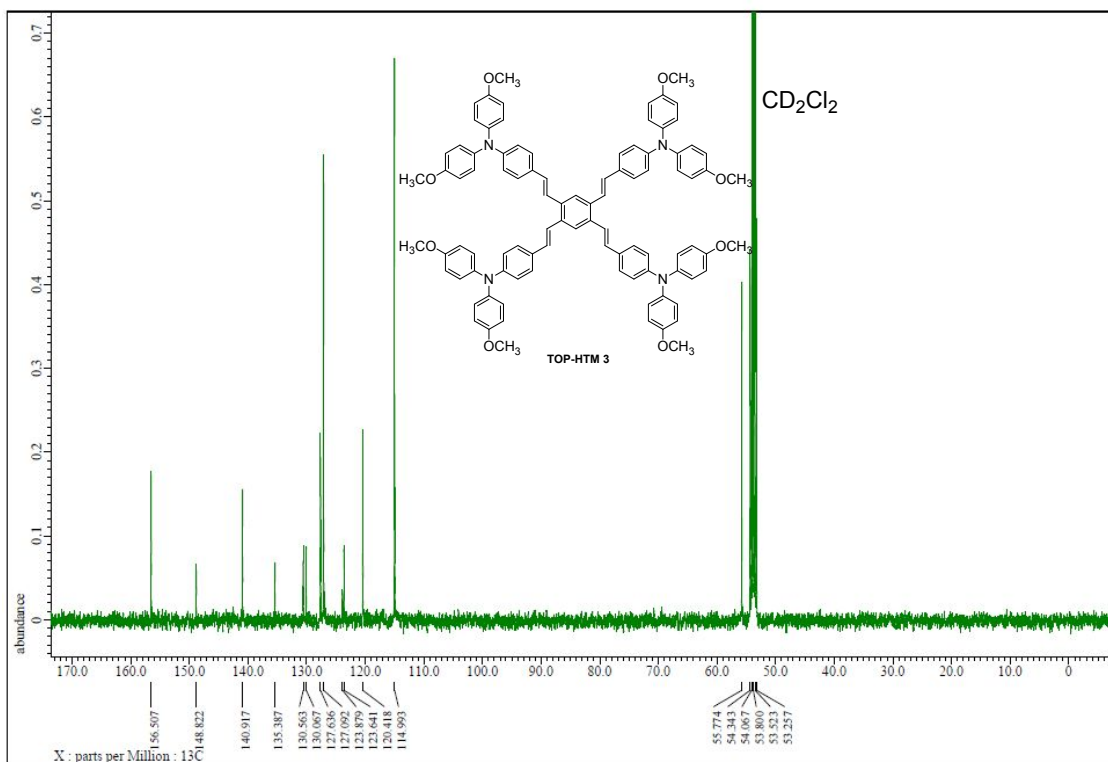


Figure S51. ^{13}C NMR of TOP-HTM **3** in CD_2Cl_2 .

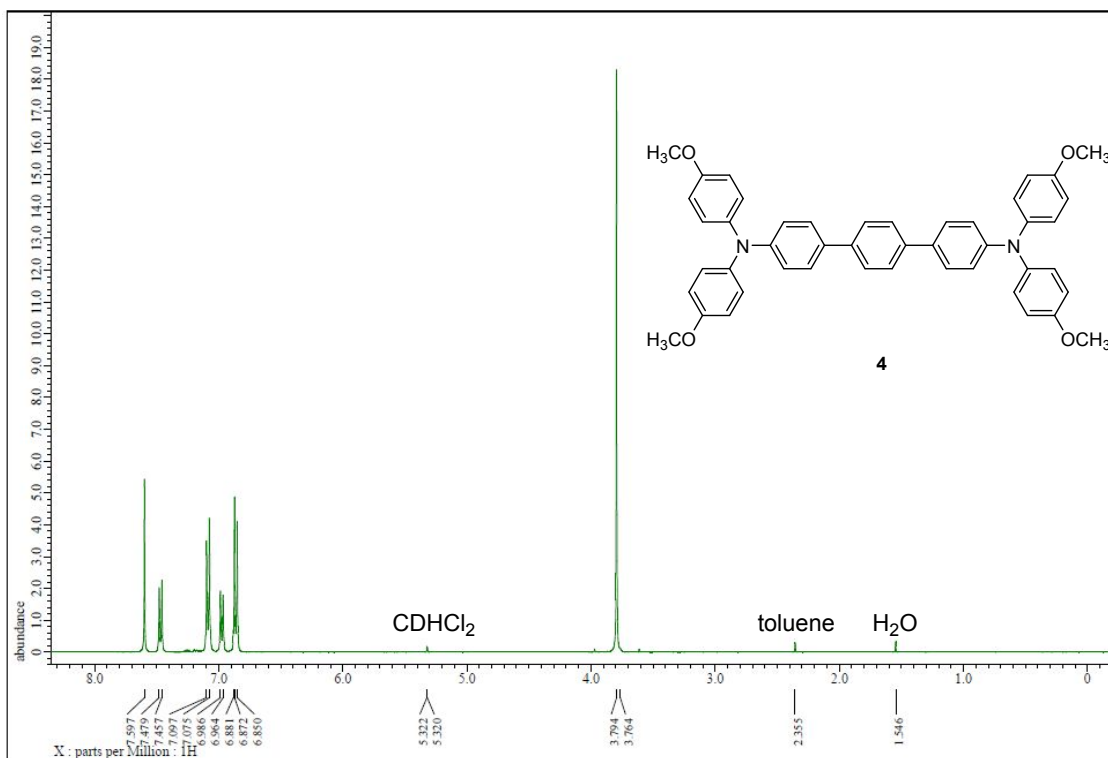


Figure S52. 1H NMR of **4** in CD_2Cl_2 .